arXiv:chao-dyn/9810007v1 1 Oct 1998

Phenomenology of Globally Coupled Map Lattice and its Extension

Tokuzo Shimada

Department of Physics, School of Science and Technology, Meiji University

Higashi-Mita 1-1, Kawasaki, Kanagawa 214, Japan

(February 5, 2008)

Abstract

We revisit the globally coupled map lattice (GCML) and also propose a new extended globally coupled map lattice (EGCML) with an inverse power law interaction. In GCML we clarify the mechanism of the basic posi-nega switch in the two-cluster regime. We show that there is a natural mechanism in GCML which guarantees no mixing of maps across their mean field in the chaotic transient process. In the turbulent regime of GCML there is a prominent period three window. In the correlator analysis we also find a remnant of periodic motion of quasi-clusters with high rate mixing almost everywhere in the turbulent regime of the large-size GCML. The so-called hidden coherence is the most modest remnant. The EGCML shares the same intriguing properties with GCML and exhibits an amazing spatial cluster formation during the chaotic transient process. An analytic approach is proposed which relates the periodicity manifestation in the turbulent regime of GCML to the periodic window of a single logistic map.

05.45.+b,05.90.+m,87.10.+e

Typeset using REVTEX

I. INTRODUCTION

Recently there has been much progress in the study of synchronization of nonlinear maps [1–4] and flows [5–10]. This may lead to the clarification of the intelligence supposed to come from the synchronization among the neurons in the neural network, e.g. [11]. Especially the globally coupled map lattice (GCML), a system of identical maps coupled via their mean field, has surprisingly rich clustering phases in the space of the nonlinearity parameter and the coupling. In the ordered two-cluster phase, GCML exhibits a posi-nega switch between clusters of synchronizing maps controlled by external inputs [1]. Furthermore even in the turbulent regime there emerges some hidden correlation which was first observed as the violation of the law of large numbers (LLN) in the fluctuation of the mean field in the time series [2,12]. GCML is a natural extension of the spin-glass models [13,14] and these interesting features may be relevant to the intelligence activity. All the maps in GCML contribute to the mean field with an equal weight and hence there is no notion of distance between maps. It is conjectured that the intriguing properties of GCLM, both the posi-nega switch and the hidden coherence, come from this bona fide scaling invariance of GCML [1,2]. However, neither the reason why there occurs complete swapping of the maps between clusters in the posi-nega switch in the two-cluster phase nor the global feature of the turbulent phase has been elucidated so far. The purpose of this article is twofold. Firstly, we revisit GCML. We show that there is a natural mechanism which guarantees the complete swapping of maps in the two-cluster posi-nega switch. The key to this mechanism is the motion of the mean field during the transient process. We show that even though whole maps are released from tightly synchronizing clusters to chaotic violent movements during the transient process, still they never mix across their mean field. We clarify the mechanism for this phenomenon. We also perform an extensive survey of the turbulent regime of GCML. We show that this regime has a prominent period three window and is full of periodicity remnants. A correlator analysis detects quasi-periodic clusters with high mixing rate among them almost everywhere in the turbulent regime of the large-size GCML.

The so-called hidden coherence occurs in-between the regions of the quasi-clusters and the valleys with no violation of LLN as the most modest appearance of the periodicity remnants.

Secondly, we construct a new extended globally coupled map lattice (EGCML). Our EGCML is a two-dimensional map lattice and the maps are under all-to-all interaction as in the GCML. But instead of the uniform interaction in GCML, the interaction in EGCML obeys an inverse power law with respect to the distance between the maps on the lattice. EGCML locates at an intermediate position between the nearest neighbor coupling map model and the GCML with uniform interaction. Thus EGCML facilitates a test whether the salient feature of GCML is due to the scale invariant interaction in it. We find that EGCML indeed inherits the intriguing properties of GCML though they turn out diffuse to some extent. For instance, in the two-cluster phase of EGCML, the two clusters follow the same bifurcation tree with that of GCML when the population unbalance between the clusters are increased but the synchronization of maps in each cluster is looser in EGCML than in GCML. We also observe in the turbulent regime of the EGCML the same periodic window as well as the quasi-periodic clusters with high mixing rate.

GCML exhibits the basic posi-nega switch as well as more intricate controlled switches among coded clusters at various hierarchical levels in its simplest construction [1] and certainly serves as a model for intelligence activity. But the very fact that it is a system of globally coupled maps with an equal coupling makes it lose the notion of the distance between maps. In a way it is a zero dimensional chaotic field theory. Apart from the intelligence one is interested to know what is the (classical) field theory of chaotic maps on the lattice at criticality. In this aspect the synchronizing maps on the lattice may be regarded as the analog of Higgs condensation in the field theory [8,9]. We can use EGCML to see the general trend how the spatial clustering of maps occurs under the scale invariant interaction on the lattice. We find that EGCML does exhibit a self-organized formation of the spatial clusters (condensation) due to the synchronization between the maps during the chaotic transient process in the switch and after it. In the EGCML switch the positive (negative) cluster becomes negative (positive) evolving in the same two-cluster attractor as before with

only a few percent change of the population unbalance between the two clusters in most of the runs. However, there occurs the mixing of maps between the clusters.

The organization of this article is as follows. In Sec. II we pay attention to two important rules in the GCML. These are the reciprocity of the couplings among the maps and an invariance rule that the maps do not change their mean field under the interaction. We then construct EGCML based on these rules. In Sec. III we compare the phase diagrams of both models and show that they are almost the same each other. In Sec. IV we analyze the two-cluster regime of both models. For the GCML we clarify how the basic posi-nega switch between two clusters in the two-cluster regime can be realized. We then turn to EGCML and investigate the switch process in it. We show that amazing spatial clusters are formed during the chaotic transient process in the switch. In Sec. V we present the results of an extensive statistical analysis over the whole turbulent regime of both GCML and EGCML. We show that even in the turbulent regime the maps are under coherence with various manifestations of periodicity effect. We conclude in Sec. VI.

II. MODEL CONSTRUCTION

The coupled map lattice model in general is a system of one-dimensional field on a lattice Λ with number of sites N which evolves simultaneously by an iteration of the following two steps:

$$\begin{aligned} x_P(n) &\longmapsto f(x_P(n)) \\ f(x_P(n)) &\longmapsto x'_P \equiv x_P(n+1) = (1-\varepsilon) f(x_P) + \varepsilon \sum_{Q\in\Lambda} J_{PQ} f(x_Q). \quad \forall P \in \Lambda. \end{aligned} \tag{2.1}$$

In the first step all x_P on the lattice (called as 'map' conventionally) are simultaneously mapped by a nonlinear function f. The function f could be different site by site but we consider here the simplest case that f is a simple logistic map $f(x) = 1 - ax^2$ common to all sites. In the second step the maps undergo interaction between themselves. The $N \times N$ constant matrix (J_{PQ}) represents the coupling between the maps at P and Q on the lattice

and the parameter ε is an overall coupling constant. Thus the model in the simplest form has only two parameters, the nonlinear parameter a and the coupling constant ε. If we rewrite (2.1) in terms of $y_P \equiv f(x_P)$, we obtain

$$y'_P = f\left((1-\varepsilon)y_P + \varepsilon \sum_{Q\in\Lambda} J_{PQ} y_Q\right), \tag{2.2}$$

which is a familiar form in the neural network analysis [13,14].

A. The globally coupled map lattice: GCML

In GCML [1] we consider N maps $x_P (P \in \Lambda)$ which evolve as

$$x'_P = (1-\varepsilon) f(x_P) + \varepsilon \langle f \rangle \ , \tag{2.3}$$

where $\langle f \rangle$ is the mean field on the lattice

$$\langle f \rangle \equiv \frac{1}{N} \sum_{Q\in\Lambda} f(x_Q). \tag{2.4}$$

Thus the coupling matrix of GCML is simply

$$J_{PQ} = \frac{1}{N}, \qquad P, Q \in \Lambda \tag{2.5}$$

and clearly satisfies the reciprocity

$$\text{(I)} \qquad J_{PQ} = J_{QP}. \tag{2.6}$$

From (2.3) and (2.4) we can also derive a relation

$$\text{(II)} \qquad \sum_{P\in\Lambda} x'_P = \sum_{P\in\Lambda} f(x_P). \tag{2.7}$$

This relation guarantees that the mean field value is kept invariant when the maps undergo the interaction at the second step of the interaction. These two relations serve as a guide to construct the map lattice models in general. Let us examine the implication of the invariance rule (II). The nonlinearity of f generally magnifies the variance among the maps. Therefore,

the first step may be regarded as a *defocusing lens* with some *random prisms* installed in it. The larger the parameter a is, the more strongly the defocusing lens acts on the system of maps. In the second step every $f(x_P)$ is pulled to the mean field $\langle f \rangle$ at a fixed rate $1-\varepsilon$. Thus the second step acts as a *focusing lens*. The larger the coupling ε is the more strongly the focusing lens acts. Since (2.3) is a conformal contraction transformation the position of the *center of mass* $\langle f \rangle$ of the system is kept invariant during the interaction. This is what the invariance condition (II) implies. Thanks to the invariance condition the fluctuation of the mean field of the maps is caused only at the first defocusing process. The maps in GCML evolve in time repeating this two-step process of defocusing and focusing. Under the battle of the two conflicting tendencies the maps eventually form an attractor in which fluctuations among maps is maximally suppressed by the averaging effect of the interaction via the mean field.

What is the condition on the coupling matrix J_{PQ} for a general map model of the form (2.1) satisfies the invariance condition (II)? By summing up (2.1) over P and using (II) we obtain a relation

$$\sum_{P\in\Lambda} f(x_P) = \sum_{Q\in\Lambda} \left(\sum_{P\in\Lambda} J_{PQ} \right) f(x_Q). \tag{2.8}$$

At any step of the iteration this must hold. Thus the necessary and sufficient condition on the coupling J_{PQ} is

$$\sum_{P\in\Lambda} J_{PQ} = 1, \quad \forall Q \in \Lambda. \tag{2.9}$$

From reciprocity (I) this is equivalent to

$$\sum_{Q\in\Lambda} J_{PQ} = 1, \quad \forall P \in \Lambda. \tag{2.10}$$

B. The nearest-neighbor coupling lattice model

This type of a model is known to show an interesting spatial cluster formation similar to the spin glass [3]. On the other hand it is also known that the interesting two features of the

GCML, i.e. the posi-nega switch and hidden coherence are lost. Nonetheless it is instructive to check that this model satisfies (I) and (II) like GCML. Let us denote the sub-lattice of Λ as λ_P which is a set of the nearest neighbor sites to P including P itself. The model is

$$x'_P = (1-\varepsilon)f(x_P) + \varepsilon\langle f\rangle \ , \tag{2.11}$$

where $\langle f\rangle$ is the mean field of the maps in λ_P at P, i.e.

$$\langle f\rangle = \frac{1}{N(\lambda)}\sum_{Q\in\lambda_P} f(x_Q). \tag{2.12}$$

The coupling matrix is then

$$J_{PQ} = \begin{cases} \frac{1}{N(\lambda)} & \text{if } Q \in \lambda_P \\ 0 & \text{if } Q \notin \lambda_P \end{cases} \tag{2.13}$$

where $N(\lambda)$ is the number of maps in the sub-lattice λ in dimension d. But if $Q \in \Lambda_P$, then $P \in \Lambda_Q$. Hence $J_{PQ} = J_{QP}$ and the condition (I) follows. Also we have

$$\sum_{Q\in\Lambda} J_{PQ} = \sum_{Q\in\lambda_P}\frac{1}{N(\lambda)} = 1. \tag{2.14}$$

and (II) follows. Note that the interaction represents a diffusion process. For instance in $d = 1$ we can rewrite (2.11) and (2.12) as

$$y'_P = f\left(y_P + \frac{\varepsilon}{3}(y_{P+1} + y_{P-1} - 2y_P)\right), \tag{2.15}$$

and the second term is nothing but the laplacian on the one-dimensional lattice.

C. An extend globally coupled map lattice: EGCML

We now wish to construct the following model. Firstly it must have all to all interaction and satisfy the relations (I) and (II) in order to have the same defocusing and focusing dynamics as in the GCML. Secondly we wish to investigate the consequence of distance dependent interaction; in particular, we wish to know to what extent the salient features of the GCML such as the posi-nega switch or the hidden coherence depend on the fact that

the model is scale invariant trivially by the absence of distance scale. Do these features disappear if the interaction between the maps decreases with distance? Certainly at the nearest interaction limit, we know neither the posi-nega switch nor the violation of the law of large numbers occurs. Most crucial case is the interaction which decreases with distance but in a power law. In contrast to the exponential law this does not introduce the length scale and yet the interaction is all to all. Thus the model we would like to construct is an extended GCML (EGCML) in which the interaction decays with a power law and satisfies the conditions (I) and (II). Below we show there is such a natural extension of GCML. In this article we choose $d = 2$ for simplicity though our construction goes through for all dimensions.

Let us denote the set of sites at distance ρ from P as $L_\rho(P)$. The symbol L is the memento of *loop* since in $d = 2$ such a set is a loop (in fact a square on the lattice space) of radius ρ around P. We denote by $N(L_\rho)$ the number of sites in L_ρ. For $d = 2$, $N(L_\rho) = 8\rho$ ($\rho = 1, 2, \cdots$) and $N(L_0) = 1$. We denote the maximal radius of the loop realized in the lattice Λ as κ. This is the perimeter of the lattice and for $d = 2$, $\kappa = [(N^{\frac{1}{2}} - 1)/2]$. To be precise we present our result for $N^{\frac{1}{2}}$ odd but we have checked no change of results occurs for $N^{\frac{1}{2}}$ even. In order to treat all of the sites in Λ democratically and to minimize the finite size effect we impose the periodic boundary conditions. For any point P on the lattice we calculate the effect of all maps within κ taking into account the periodic boundary condition. The EGCML is then compactly described as

$$x'_P = (1 - \varepsilon) f(x_P) + \varepsilon \langle\langle f \rangle\rangle_P. \tag{2.16}$$

where $\langle\langle f \rangle\rangle_P$ at P is given by

$$\langle\langle f \rangle\rangle_P = \frac{1}{\kappa} \sum_{\rho=0}^{\kappa} \langle f \rangle_{P,\ \rho} \tag{2.17}$$

$$\langle f \rangle_{P,\ \rho} = \frac{1}{N(L_\rho)} \sum_{Q \in L_\rho(P)} f(x_Q). \tag{2.18}$$

In words the effect of all the maps on the lattice to the map at P is determined by a double average. Firstly any one of the maps at an equal distance ρ from P must affect the map

at P with the same weight. Thus they are averaged with an equal weight and this gives $\langle f\rangle_{P,\,\rho}$. Then, the effects of maps with various distances from P must be accounted for. In the EGCML this is done again by taking an equal weight average of $\langle f\rangle_{P,\,\rho}$ over ρ from zero to κ which gives $\langle\langle f\rangle\rangle_P$ as a natural non-local extension of the diffusion process. The first average must be an equal weight average to respect the rotational symmetry. The second average must be again an equal weight average. It is necessary for the invariance condition (II) as we show below.

The coupling matrix element J_{PQ} is the weight factor for the $f(x_Q)$ to contribute to x'_P via the double average and is given by

$$J_{PQ} = \frac{1}{\kappa N(L_\rho)} \;\propto \rho^{-(d-1)} \qquad \forall P \in \Lambda, \quad Q \in L_\rho(P). \tag{2.19}$$

Thus in EGCML any map $f(x_Q)$ at equal distance ρ from P contributes with an equal weight to the mean field $\langle\langle f\rangle\rangle_P$ and the interaction decreases with an inverse power with respect to ρ for $d = 2$. The reciprocity (I) follows just as in the nearest neighbor case since $Q \in L_\rho(P)$ is equivalent to $P \in L_\rho(Q)$. Also the invariance condition (II) can be proved as:

$$\begin{aligned}\sum_{Q\in\Lambda} J_{PQ} &= \sum_{\rho=0}^{\kappa} \sum_{Q\in L_\rho(P)} J_{PQ} \\ &= \sum_{\rho=0}^{\kappa} \frac{1}{\kappa} \left(\sum_{Q\in L_\rho(P)} \frac{1}{N(L_\rho)} \right) \quad = \quad 1\end{aligned} \tag{2.20}$$

III. PHASE STRUCTURE OF GCML AND EGCML

The GCML phase diagram in the $a - \varepsilon$ plane given in [1] is reproduced in Fig. 1a to facilitate the comparison with the EGCML phase diagram. For GCML we analyzed statistically the cluster composition of $N = 1000$ maps in the final attractor from 1000 random initial configurations and we verified the original phase diagram. The various phases are the outcome of the battle between chaotic motions of maps (the defocusing effect) and the interaction via the mean field forcing the maps to move coherently (the focusing lens effect). Since the GCML phase structure is elucidated in ref. [1] we recapitulate here only

the essential features necessarily in the following discussion. Let us consider a line at $a = 1.8$ for definiteness which is well-beyond the critical value $a = 1.401$ of a single logistic map to the chaos [16]. For a sufficiently large ε (≥ 0.38) the maps in the final attractor are strongly bunched together in a cluster and evolve as a unity in the same chaotic motion as that of one single logistic map. This is the coherent phase. For ε in the range $[0.22, 0.31]$ the interaction via the mean field can no longer exerts strong bunching and the final maps divide into two clusters. The maps in each cluster are still tightly synchronizing each other, while the two clusters mutually oscillate opposite in phase. This is as a solution of a minimum fluctuation in the mean field. We discuss this ordered two-cluster phase extensively in Sec. IV.

For smaller ε, the number of final clusters increases but the number of clusters at a given ε does not depend on the number of maps N. The typical number of clusters at various ε ranges is indicated in the phase diagram. For further smaller ε (≤ 0.15) the binding of the maps is almost resolved and the number of clusters is proportional to N. This region is the turbulent phase and we extensively analyze this regime in Sec. V. Final remark is that the boundary values of ε between phases simultaneously increase (decrease) in order to maintain the balance between the conflicting tendencies if the coupling a is increased (decreased).

We show in Fig. 1b the corresponding phase diagram of the EGCML. We used 39×39 map lattice and analyzed statistically the final attractor configuration using typically 200 runs for each (a, ε).[1] There is a remarkable agreement between two phase diagrams except for slight shifts in the phase boundaries. For instance, for the EGCML at $a = 1.8$, the coherent phase, the ordered two-cluster phase, and the turbulent regime are respectively realized at $\varepsilon \geq 0.38$, $0.22 \leq \varepsilon \leq 0.31$ and $\varepsilon \leq 0.15$ to be compared with the boundaries

[1] We note that the EGCML run requires increasingly large computation time for large-size lattice since the $\langle\langle f \rangle\rangle_P$ for each map at the lattice site P must be individually calculated using the inverse power law. For $N = 39^2$ EGCML, the necessary CPU time is about a hundred times of that for GCML of the same size.

quoted above. This agreement between two phase diagrams indicates strongly that EGCML is in the same universality class [17] with GCML.

IV. THE POSI-NEGA SWITCH IN GCML AND THE PATTERN FORMATION IN EGCML

A. The Two-Cluster Regime and the θ Variable

The ordered two-cluster phase of GCML is realized in a band in the a, ε parameter space with $\epsilon \in [0.2, 0.23]$ at $a \approx 1.6$ and $\epsilon \in [0.28, 0.33]$ at $a \approx 1.98$ (see Fig. 1a) . In this phase, the maps divide into two clusters after some transient steps for most of the initial values. The clusters oscillate around the unstable fixed point x^* mutually opposite in phase and the maps in each of the two clusters are in tight synchronization. In order to distinguish the two clusters we follow the convention in [1] and name the cluster which takes a value above (below) x^* at an even step n from the first of the iteration as the positive (negative) cluster. We denote the number of maps in the positive (negative) cluster as $N_+(N_-)$ and define the population ratio parameter $\theta \equiv N_+/N$. The values of maps in the positive (negative) cluster are uniformly x_+ (x_-) if the synchronization of maps in each cluster is really tight. The maps are evolving in two clusters repeating the two step process of mapping and interaction and the dynamics of maps is reduced to that of two clusters:

$$x_\pm(n) = (1-\varepsilon) f(x_\pm(n-1)) + \varepsilon \langle f(n) \rangle \tag{4.1}$$

and the mean field of maps at time n is given by

$$\begin{aligned} \langle f(n) \rangle &\equiv \frac{N_+}{N} f(x_+(n-1)) + \frac{N_-}{N} f(x_-(n-1)) \\ &= \theta x_+(n) + (1-\theta) x_-(n) \\ &= \langle x(n) \rangle \end{aligned} \tag{4.2}$$

where the second equality comes from the invariance condition (II) for the two-cluster configuration. Thus when a set of three numbers, a, ε and θ is given the attractor of the two

clusters is uniquely determined. For the discussion of the posi-nega switch below let us explain these by an explicit sample in Fig. 2. In the left box we illustrate the mechanism of Eqs. (4.1) and (4.2) and in the right box we show a sample attractor of two clusters realized at $a = 1.98$, $\varepsilon = 0.3$ and the corresponding motion of the mean field. The two clusters, represented by white and black circles, evolve in time under the iteration of mapping (solid arrows) and focusing by interaction (dashed arrows). The mean field (a short bar) is kept invariant under the interaction as dictated by the invariance condition (II) and (4.2). The first time n_0 in this run happened to be even. Hence the positive cluster is the white circle moving as $(+ - + \cdots)$ and the negative one is the black circle moving as $(- + - \cdots)$. We see that they move in period four and mutually opposite in phase. The mean field is closer to the negative cluster, which means that the positive cluster is the minority cluster and θ must be less than half. Numerically $\theta = 0.43$ for this attractor. Note that it is probabilistic whether the first time n_0 is even or odd. From another initial configuration the same attractor *modulo translation in time* may be equally realized. If the translation is odd steps in time we will have the same figure but with n_0 is now odd. The dominant cluster (black circle) must be then named as the positive cluster and $\theta = 0.57$ by definition.

In Fig. 3a and b we show the attractors of GCML and EGCML at $a = 1.98$ and $\varepsilon = 0.3$ respectively as a function of θ. We used 10^3 runs for GCML and 4×10^3 runs for EGCML. In one run for GCML, $N = 1000$ maps are iterated from a random initial configuration and to account for the first transient process the values of maps during the 512 steps after the first 10^4 iteration are plotted at the fraction of maps with $x_i(n) > x^*$. For instance the run shown in Fig. 2 with n_0 even contributes four points $(1, 1^*, 3, 3^*)$ at $\theta = 0.43$ and other four points $(2, 2^*, 4, 4^*)$ at $\theta = 0.57$. Then the run is repeated and the results of all runs are superposed in order to see the dependence of the attractor on the population unbalance between the clusters. Note that this is equivalent to plot the maps only at the last even iteration steps at θ when the results from many initial configurations are superposed. The GCML attractor in

Fig. 3a agrees with that found in ref. [1] [2]. When θ approaches an upper threshold θ_{th} from below (or a lower threshold $1-\theta_{th}$ from above) the attractor undergoes successive period doubling and at the thresholds the maps fall into chaos (θ_{th}=0.63 and $1-\theta_{th}=0.37$ for $a=1.98$).

For EGCML in Fig. 3b the final attractor of $N=51\times 51$ maps is measured in a similar way but in order to shorten the large computing time necessary for EGCML a routine is included in the iteration program which judges whether the maps have fallen into a periodic attractor of a certain period T less than or equal to 2^6 or not[3]. If the judgment condition is satisfied the maps are plotted at the fraction of maps with $x_(n) > x^*$ only during the next one cycle of the attractor and the next run is started. This not only shortens the calculation time but also enables the statistical analysis of the frequency of the occurrence of the attractors and of the fluctuation of maps in a given attractor since indefinitely duplicated plotting of the maps is avoided. If on the other hand the maps do not fall into an attractor all through the 10^4 steps the maps are plotted for the next 512 steps just as in the GCML run. In EGCML we find that the maps in a cluster synchronize more loosely than those in GCML. The dispersion of maps in each cluster is approximately 0.1 for all θ to be compared with the gap size ≈ 1.0 between the two bands of the attractor at $\theta \approx 0.5$. Even though the maps do not mix between the clusters in the final stable attractor this fluctuation hides the details of bifurcation structure with respect to θ in a direct superposition of all runs in terms

---

[2]We note that the lower half attractor of GCML in [1] is erroneously a mirror image of the correct one.

[3] In the iteration N_+ is calculated at every even step n and when it stops to vary during ten successive steps the routine is activated at n_0. It calculates the judgment condition $\sum_i (x_i(n_0+T)-x_i(n_0))^2 < 10^{-6}$ and if this is satisfied for some $T(\leq 2^6)$ the maps are judged to have fallen into an attractor of a period T. If not, the routine is inactivated and the next stabilization of N_+ is waited for.

of the bitmap graphics. Thus we have done a statistical analysis of the plot density and removed those points with density less than one percent of the maximum density from the diagram. This procedure is justified because we truncated each run just after one cycle of the periodic attractor so that each run contributes to the points on the attractor diagram with an equal weight. It was a remarkable instance in this work when we observed the same bifurcation diagram with GCML turned out in the central region of the EGCML attractor ($\theta \in [0.38, 0.62]$) as is shown in Fig. 3b. In EGCML the synchronization of maps in a cluster becomes looser than that of GCML but still the dynamics of final clusters is common for both GCML and EGCML and controlled by θ. We have already seen above that EGCML is endowed with a phase diagram remarkably similar to that of GCML and now we find that the attractors in both models in the ordered two-cluster regime are also similar.

The posi-nega switch in GCML uses the ability of θ to control the attractor. But before delving into the detail discussion of the posi-nega switch let us examine to what extent the reduction of dynamics of maps is realized. If the reduction is really effective down to two degrees of freedom, all $N_+(N_-)$ maps in the positive (negative) cluster should have a single value $x_+(n)$ $(x_-(n))$. Then Eqs. (2.3) and (2.4) should reduce to (4.1) and (4.2) or equivalently to a matrix coupled two-map model

$$x'_+ = (1-\varepsilon_-)f(x_+) + \varepsilon_- f(x_-), \tag{4.3}$$
$$x'_- = (1-\varepsilon_+)f(x_-) + \varepsilon_+ f(x_+),$$

with $\varepsilon_+ = \varepsilon\theta$ and $\varepsilon_- = \varepsilon(1-\theta)$. From the remarkable agreement between GCML attractor (Fig. 3a) and two-map model attractor (Fig. 3c) we see that in the two-cluster phase of GCML the dynamics of the N maps reduces to that of two maps for all θ between the thresholds.

In EGCML the coupling J_{PQ} is not a single constant but it depends on the distance between $P$and Q. The interaction acts on a map at a site P via the position dependent mean field $\langle\langle f\rangle\rangle_P$ which is a double sum given by (2.17) and (2.18) contrary to a single sum $\langle f\rangle$ given by (2.4) in GCML. Therefore the reduction of EGCML to two maps we find

in Fig. 3b requires an explanation. What is important here is not the uniformness of the couplings but the scale invariance of them. In both GCML and EGCML the interaction has no cutoff scale and hence it prevails over the lattice and the maps are forced to synchronize among themselves due to the averaging effect of the interaction via the mean field. Thus the possible difference of EGCML from GCML comes solely from the variation of the site dependent $\langle\langle f\rangle\rangle_P$ around $\langle f\rangle$. If the variation is small both models will show similar attractors. EGCML is constructed in such a way to assure this small variance when the interaction forces the maps to synchronize.

First let us consider a simple case where the nonlinear parameter a is so small that the chaotic randomness in each map cannot overcome the averaging effect. Then after iterations all the maps on the lattice will synchronize and take approximately the same values with only a small variance. If we ignore this variance, the value $f(x_P)$ common to all P becomes a multiplicative factor to the sum for the mean field and $\langle\langle f\rangle\rangle_P = \langle f\rangle$ follows from the invariance conditions (2.9) for GCML and (2.20) for EGCML. In GCML the variance is negligible but in EGCML the weaker synchronization causes a variance typically to the order 10^{-2} in $\langle\langle f\rangle\rangle_P$ and the EGCML attractor turns out reflecting this variance. But otherwise EGCML behaves just like GCML.

Now in the two-cluster phase at higher a the maps cannot be bunched together in a single cluster and divide into two clusters, A and B. The maps in each of the clusters take approximately the same value and synchronize among themselves. Hence we may write

$$x_i = X_A + q_i \quad (i \in A)$$
$$x_j = X_B + q_j \quad (j \in B)$$

Here X_A (X_B) is the collective coordinate for A (B) (the average of maps taken over A (B) only) and the q_i (q_j) represents small fluctuation around the X_A (X_B). Now let us analyze $\langle\langle f\rangle\rangle_P$ for EGCML. An important observation is that the double sum for $\langle\langle f\rangle\rangle_P$ can be written as a sum of two double sums, one only over cluster A and the other only over cluster B. This decomposition allows one to apply the above argument to each of the clusters and

the $f(X_A)$ ($f(X_B)$) becomes a multiplicative factor to the double sum for cluster A (B). As for the remaining double sum of couplings, some more consideration is necessary. In EGCML a 'polarized' distribution of maps is in principle allowed in which, for instance, the maps in the cluster A (B) accumulate around a given point P and maps in cluster B (A) accumulate far from P. But EGCML has no interaction to induce such a polarization and the randomness in each map also acts to break the polarization. We have numerically checked the dominance of unpolarized distributions. Therefore the remaining double sum for EGCML again counts the number of maps in each cluster just in the same way the single sum for GCML does in (4.2). Thus we have also in EGCML

$$\langle\langle f\rangle\rangle_P \approx \frac{N_A}{N} f(X_A) + \frac{N_B}{N} f(X_B) \tag{4.4}$$

Here the approximation takes into account both the polarization in fluctuation and the small variance of maps in each cluster due to approximate synchronization. Thus the collective coordinates X_A and X_B of the clusters is described by the matrix coupled two-map model and the maps in each of the clusters fluctuate around the collective coordinates. This explains the approximate reduction of EGCML to two maps.

B. A resolution of the posi-nega switch mechanism

The posi-nega switch found in GCML [1] is based on the ability of θ as the control parameter of the GCLM attractor. If maps are successively transported from one cluster to the other by input ($x_i \longrightarrow x_i \pm \delta$) the population unbalance can be enhanced and the attractors undergo successive bifurcation. When θ reaches the threshold the whole maps go into a grand chaotic motion almost bunched together in a unit. See Fig. 4 for a typical sample of this transition. This state induced by an excess of the last one map is unstable as we see in Fig. 3a that there is no self-organized stable attractor above θ_{th} (or below $1-\theta_{th}$). Thus after some transient time the maps again form the allowed stable configuration, that is, tightly bound two clusters mutually oscillating opposite in phase. Just as before let us

again label the new cluster as positive if it takes a value above x^* at even step n (counting from the start of iteration) and the other as negative. An amazing finding in [1] is that the composition of the new two clusters is limited only in two ways. (1) All the maps involved in the positive cluster before the chaotic transient are now involved in the negative cluster. (2) All the maps in the old positive cluster are again in the new positive cluster. The case (1) is the posi-nega switch. In both cases the maps behave as if they keep a *memory* of their former clusters. But how is it possible? The maps pass the chaotic transient process where many two-cluster states as well as many other channels are open. What is the mechanism that protects the maps from mixing?

Before answering this old puzzle let us point out some trivial aspects of the posi-nega switch. First there is no essential difference between case (1) and (2). How long the chaotic transient process persists and in particular whether the duration time is even or odd is (almost) probabilistic. It is of course deterministic but highly dependent on the map values at the onset of the transient process. Whether a cluster after the transition is positive or negative depend on the parity (even or odd) of the duration time by definition and there is no sense to distinguish (1) and (2) when the parity is indefinite. Second we should note that in the two-cluster phase of GCML with fixed a and ε the self-organized attractor is determined solely by the population unbalance between the two clusters. In case (1) $\theta \longrightarrow 1-\theta$ and in case (2) $\theta \longrightarrow \theta$. In either case, the population *unbalance* is the same before and after the transition and hence the attractor before and after must be the same. To be precise, to put the attractor before the transition upon that after the transition we need a temporal translation of odd steps in case (1) and even steps in case (2). Modulo this difference the attractor before and after the transition are the same in either case. There is no chance of appearance of a new attractor *provided that* the population *unbalance* before and after the transition is the same [4]. Therefore the real puzzle boils down to a

[4]In ref. [1] this point that the maps come back to the same attractor is not noted.

single question. What is the mechanism which keeps the population unbalance between two clusters unchanged before and after the chaotic transient process? We solve this puzzle below in two steps. First we discuss how the chaotic transient process starts and ends. This provides the temporal boundary conditions of the transient process. Then we show there is a very simple mechanism which transfers the population unbalance rate through the transient process.

1. The transition at the threshold

The logistic map $f(x)$ copies the region $[-x_L, x_L]$ onto itself twice-fold as follows[5].

$$[-x_L, x_L] \equiv I + II + III$$

$$I \equiv [-x_L, 0] \xrightarrow{f} I + II + III$$

$$II \equiv [0, x^*] \xrightarrow{f} III$$

$$III \equiv [x^*, x_L] \xrightarrow{f} II + I \ .$$

The first two mappings are monotonously increasing while the last is monotonously decreasing. See Fig. 5. Below the threshold the two clusters are moving mutually opposite in phase around x^* so that one must be in region III and the other in region I or II. When the unbalance is increased by sending the maps of the minority cluster to the majority cluster the mean field comes closer to the majority cluster and oscillates in phase with it. The interaction conformally contracts the maps to the mean field at every iteration step, and the minority cluster is pulled to the mean field more strongly at this highly unbalanced situation. In a few iterations after the unbalance exceeds the threshold by the last input,

[5] For the map $f(x) = 1 - ax^2$ the limits are $\pm x_L = \pm(1 + \sqrt{1 + 4a})/2a$ and the unstable fix point is $x^* = (-1 + \sqrt{1 + 4a})/2a$ but the argument here is independent of the particular parametrization of the map. All we need is the universal folding nature of the map.

the non-dominant cluster crosses the boundary x^*. This is the very time of the start of grand chaotic transient motion of maps. At the next step of iteration all maps must move into the same direction. The synchronization opposite in phase ceases and the maps start almost coherent evolution. The mean field evolves together in the middle of them. The focusing effect of the interaction now works only to bunch the maps close together around the mean field. The high nonlinearity of each map then becomes manifest and all maps move around the three regions bunched together in a pseudo-cluster with a slight variance around their mean field. In the typical sample run shown in Fig. 4 the mean field (depicted by a short sold bar) oscillates closely to the dominant cluster (connected by the solid line) for several steps. At time n_1 the minority cluster (the dashed line) is pulled down across the x^* and at the next step both clusters are mapped upwards together. Then the grand chaotic motion starts at n_2. The pseudo-cluster is formed by the external input and is unstable. To bunch it stably the coupling must be larger; it must have the value for the coherent region (e.g., $\varepsilon > 0.43$ for $a = 1.98$). The tiny variance between maps in the pseudo-cluster is soon magnified and the transient pseudo-cluster is broken to the self-organized stable two clusters again. In the following we use the fact that the maps starts and exits the transient process with small variance among them.

2. The population conservation mechanism during the chaotic process

Let us define the relative coordinates $\tilde{x}_i$ with respect to the mean field

$$\tilde{x}_i(n) \equiv x_i(n) - \langle x_i(n) \rangle, \tag{4.5}$$

$$\langle x_i(n) \rangle \equiv \frac{1}{N} \sum_{i=1}^{N} x_i(n). \tag{4.6}$$

Since all of the maps are now close to the mean field we may expand $f(x_i(n))$ as

$$f(x_i(n)) = f(\langle x_i(n) \rangle) + \tilde{x}_i(n) \left. \frac{df}{dx} \right|_{\langle x_i(n) \rangle} + O(max(\tilde{x}_i^2)). \tag{4.7}$$

Averaging this over i using $\sum_{i=1}^{N} \tilde{x}_i(n) = 0$ we obtain a relation

$$\langle f(x_i(n))\rangle \equiv \frac{1}{N}\sum_{i=1}^{N} f(x_i(n)) = f(\langle x_i(n)\rangle) + O(max(\tilde{x}_i^2)). \tag{4.8}$$

But the interaction does not affect the mean field (the condition (II)). So we obtain

$$\langle x(n+1)\rangle = \langle f(x_i(n))\rangle = f(\langle x_i(n)\rangle) + O(max(\tilde{x}_i^2)). \tag{4.9}$$

Therefore the evolution equation of the relative coordinates is given by

$$\begin{aligned}
\tilde{x}_i(n+1) &\equiv x_i(n+1) - \langle x_i(n+1)\rangle \\
&= \Big((1-\varepsilon)f(x_i(n)) + \varepsilon\langle f(x_i(n))\rangle\Big) - \Big(f(\langle x_i(n)\rangle) + O(max(\tilde{x}_i^2))\Big) \\
&= (1-\varepsilon)\Big(f(x_i(n)) - f(\langle x_i(n)\rangle)\Big) + O(max(\tilde{x}_i^2)) \\
&= (1-\varepsilon)\frac{df}{dx}\bigg|_{\langle x_i(n)\rangle} \tilde{x}_i(n) + O(max(\tilde{x}_i^2)).
\end{aligned} \tag{4.10}$$

We used (4.8) once more in order to derive the third line.

The last line is crucial. The factor $(1-\varepsilon)df/dx\,\big|_{\langle x_i(n)\rangle}$ is common to all maps and in particular it acts with a common sign. Thus at every step in the chaotic transient process the maps separated by the mean field never mix each other. This is the mechanism which keeps the population unbalance unchanged before and after the chaotic transient process. The sign of the factor at n depends on the mean field value $\langle x_i(n)\rangle$. Hence case (1) and (2) may occur equally. We note that the invariance condition (II) is used in proving the mechanism. This condition is really important to explore the model which shares the property of GCML.

In the above resolution we examined the case in which the maps are confined in a pseudo-cluster and their variance around the mean field is kept small due to synchronization. Numerically we can trace the motion of the pseudo-cluster. Almost always the maps moves in a pseudo-cluster around the mean field with squared variance less than 10^{-4}. But sometimes it intermittently splits into two or more tight clusters around the mean field. This does not invalidate above resolution. The danger of the mixing of members between clusters occurs only when they come close each other. Our mechanism gives a guarantee that no mixing occurs even in such emergence.

C. Numerical tests of the GCML posi-nega switch mechanism

In Fig. 6a we show a posi-nega switch in $N = 60$ GCML $(a = 1.98, \varepsilon = 0.30)$. In the upper (lower) diagram the maps at the even (odd) iteration steps are plotted and connected by lines. A similar figure was given in the first report of the GCML switch [1] but the evolution of maps only at the even iteration steps was presented. By such a diagram only it looks as though the attractor undergoes a transition to a new periodic attractor after the posi-nega switch. But as we noted above, the attractor before and after the switch is the same modulo temporal transport of odd steps. We can see clearly in Fig. 6a the attractor on the whole, the even and odd iteration steps together, is precisely the same before and after the chaotic transition. As indicated by the arrows the switch from positive to negative is trivially a change in the count (even or odd) of iteration steps. What is not trivial is that the memory of the composition of two clusters is kept during the posi-nega switch. In Fig. 6b we present a posi-nega switch event of $N = 50$ GCML at even iteration steps only as a three-dimensional landscape plot. The peaks (valleys) before the chaotic transient process become the valleys (peaks) which is the posi-nega switch. In the transient process the maps form a surface which is chaotically oscillating but at any instance the segment of the surface looks remarkably horizontal. This shows that in the transient process the maps are in quasi-coherent motion with only a tiny variance. In Fig. 6c we show a *print circuit pattern* of the same switch event only at even iteration steps distinguishing the maps with respect to the mean field value. Those maps with $(x_i(2n) > \langle x(2n) \rangle)$ are shown with white squares and the others by black squares. Just as we proved above, the pattern clearly shows that there is no mixing of maps across the mean field all through the switch event. It can be also seen in Fig. 6c that the transient process ceases when the last transferred map $(n = 12)$ comes back to its home cluster. This is a typical way of the end of GCML switch. This completes our resolution of the posi-nega switch mechanism.

D. The spatial cluster formation in the EGCML switch

The EGCML has almost the same phase diagram with GCML as we showed in Sec. III and the attractor of EGCML in the two-cluster phase has the same bifurcation tree structure with that of GCML. But as we showed in Fig. 3b the attractor of EGCML turns out with some variance. That is, the dynamics of clusters in EGCML is reduced to that of matrix-coupled of two maps just as in GCML but the maps in each EGCML cluster are in phase-synchronization rather than in tight synchronization in contrast to GCML. The all to all interaction with no cutoff scale in EGCML is effective enough to maintain the reduction to two-cluster dynamics for any θ between $[1-\theta_{th}, \theta_{th}]$.

In the numerical simulation of EGCML we find that the two clusters of EGCML undergo a switch process by inputs which is similar to that in GCML. A typical sample of the EGCML switch is shown in Fig. 7. But let us first list the general differences of EGCML switch from GCML switch below and add description particular to Fig. 7 afterwards.

(1) *Slower Reaction* : By an injection of a pulse we transfer a map in the minority cluster to the majority cluster. In GCML the reaction of the attractor to this input is quite rapid and the attractor shifts to the new movement only after a few steps of the iteration. On the other hand in EGCML the attractor reacts to the input gradually in several iteration steps. This has a simple reason. The synchronization of maps in an EGCML cluster is looser. When a map is transferred there occurs a negotiation among maps in each cluster to reform the clusters and then the two clusters mutually move to the new attractor. This is similar to the two step phase-synchronization found in the globally coupled flows [8,9].

(2) *Self-Organized Transition* : In EGCML the effect of one pulse depends on the unbalance between clusters at the time of injection. If the unbalance is not high just a slow reaction of the attractor described above occurs. If the unbalance is high the map transportation by an input is followed by a self-movement of another map between clusters in the same direction. This occurs after a few tens of steps for the EGCML of the size $N \approx 10^3$. If the unbalance is close to the threshold determined by the above statistical analysis (Fig. 3b) the

transportation of a single map triggers a cascade. The last injected pulse induces follower maps to move from a cluster to the other cluster in the same direction and in some 100 iteration steps the move grows up to a series of avalanches at various scales. The corresponding change of the spatial distribution of positive and negative clusters is similar to a percolation transition. Under this process no more external input is given and the maps are themselves forming a metastable state. Both the existence of a threshold and the formation of clusters at various scales suggest a remarkable similarity to the self-organized criticality, e.g. [15], but further investigation on a larger size lattice, in particular the measurement of the critical exponent, is required to verify the relation.

(3) *The Mixing* : In EGCML the two-cluster attractor after the chaotic transient process is for most cases approximately the same with that before. The change of the population unbalance is only a few percent in most of the runs. But there occurs swapping of maps between clusters and the composition of the clusters in terms of maps is often different before and after the EGCML switch. The posi-nega switch in GCML is realized by the fact that no mixing of maps across the mean field occur during the chaotic transient process. In EGCML the mixing does occur since each map is under the influence of position-dependent $\langle\langle f\rangle\rangle_P$. Thus the EGCML switch is a posi-nega switch as a cluster process but not as the map process. In view of the brain dynamics this difference may be immaterial since what is important is the activity of whole neurons rather than the identity of individual neurons.

(4) *Self-Organized Spatial Clusters in EGCML* : Before the switch the maps in the positive cluster and those in the negative cluster are almost randomly distributed on the lattice. The transition to chaotic transient process goes like a percolation transition. When the self-organized mass movement starts, the positive maps form several large-size spatial clusters and so do the negative maps. Since these spatial clusters are formed by the long-range interaction the formation of them is more remarkable in the lattice of larger size. The spatial clusters can be best traced in the chaotic process by distinguishing the maps by the mean field of whole maps. At short time scale often we observe a posi-nega switch of spatial patterns. But due to mixing the spatial clustering pattern changes at longer time scale.

Now we explain Fig. 7a which is a typical EGCML switch event sampled in 25×25 lattice ($a = 1.9, \varepsilon = 0.3$).

Preparation: The maps are iterated from random start and a few tens of pulses are injected during the first 1500 iteration steps until the two synchronizing clusters exhibit period 32 oscillation mutually opposite in phase.

Start of Chaotic Process: At $n = 1630$ we injected ten pulses simultaneously to randomly chosen maps on the lattice. This was necessary to show the whole process in one figure. Had we injected the pulses one by one with say a hundred steps in between we had been able to see the accelerated cascade transition as described in (2) above. But still we can see in Fig. 7a that the process after $n \approx 1700$ is a self-organized cascading process.

The Posi-nega Switch between Clusters: At $n \approx 2400$ the transient process ceased and a periodic attractor of two clusters appeared. As indicated by arrows we see clearly that it is the same attractor as before. The change of the unbalance of population between the two clusters is less than one percent in this switch.

The Spatial Clusters: The snap-shot patterns of the maps at the even iteration steps are shown in the boxes below the evolution plot. In the upper boxes we distinguish the maps with respect to the mean field while in the lower boxes we used the unstable fixed point x^*. In either way we can see that spatial clusters are formed by the self-interaction of maps during the chaotic transient process. We see clearly that the maps undergo a posi-nega switch among themselves between snap-shots 4-7 in the upper boxes. On the other hand in the lower boxes the pattern becomes sometimes totally black and sometimes totally white. Hence, we see that the distinction by the mean field is a better way to sense the spatial cluster formation on the lattice. A distinction by the mean field is sensitive to the fluctuation around the collective coordinate. The clustering pattern extracted by this method is the long-range fluctuation dynamics of maps on the lattice.

This long-range interaction dynamics can be seen more remarkably on a larger lattice which allows the formation of the spatial pattern of longer wavelength. In Fig. 7b we show the samples of amazing spatial patterns formed during the chaotic transient process in the

run of 61×61 lattice ($a = 1.98, \varepsilon = 0.3$). The snap-shots were sequentially taken at every four iteration steps. We observe that a small seed of fluctuation tends to grow into a circular dense pattern by the chaotic diffusion process on the lattice in accord with the isotropic interaction in EGCML. It is interesting to note the similarity of the patterns observed on the lattice to the galaxies in the universe and in particular the appearance of patterns like globular nebula. The EGCML may be used as a toy model for the formation of density fluctuations in a nonlinear diffusion process, though further study is required to test this speculation.

V. THE TURBULENT REGIME OF GCML AND EGCML

The turbulent regime is generically the region of small ε and known by the so-called hidden coherence phenomenon. Generally it is understood that in this region maps evolve almost randomly at small lattice size N and that there occurs the hidden coherence at large N. But actually the turbulent regime has a subtler feature. We are going to show that it is a regime where the grand periodic or quasi-periodic motion of the whole maps is in action almost everywhere. But first let us quote briefly previous observations in the literature in three items.

(i) When GCML is iterated from a random configuration with a small coupling ($\varepsilon < 0.2$) and a large nonlinear parameter ($a > 1.6$) it reaches a final state which is an ensemble of maps and tiny clusters, each moving chaotically due to high nonlinearity of the map. (We show below that they are under certain coherence almost everywhere in the turbulent regime even though each element looks in an independent random motion.) The number of elements increases proportionally to the number of whole maps in sharp contrast to the ordered regime where the dynamics of maps reduces to that of a few clusters [1].

(ii) It was found in the statistical analysis of the mean field fluctuations that there emerges certain coherence between elements for large lattice size N [2]. (We show below some reservation is necessary to this statement.) Let us denote the mean field of the N

maps on the lattice Λ at time n as

$$h_n \equiv \frac{1}{N}\sum_{i\in\Lambda} x_i(n) = \frac{1}{N}\sum_{i\in\Lambda} f(x_i(n-1)). \tag{5.1}$$

If $x_i(n)$ $(i = 1, \cdots N)$ are really N independent random variables with a common distribution, the mean square deviation (MSD) of the fluctuation $(\delta h^2 = \langle h^2\rangle - \langle h\rangle^2)$ should decrease proportionally to $1/N$ by the law of large numbers (LLN) and the distribution of the h_n must be a gaussian for sufficiently large N by the central limit theorem (CLT). However the time series analysis of the mean field fluctuation shows that there is a threshold N_δ in N (depending on both a and ε) above which MSD ceases to shrink even though the distributions remains in a gaussian shape. Even though the elements (maps and tiny clusters) look evolving independently each other the violation of LLN must reflect some hidden coherence between the elements. In fact an introduction of a very small independent noise term in each map restores LLN [2,12].

(iii) This violation of LLN observed in the time averaged distribution of h_n reflects that the probability distribution $\rho(x)$ that a map takes a value x explicitly depends on time. A noise intensity analysis of ensembles successfully proves LLN [12]. If LLN should hold in the time average, $\rho(x)$ would have to be the fixed point distribution of the Frobenius-Perron(FP) evolution equation [18]. It has been shown that the fixed point distribution is unstable due to the periodic windows inherent to the chaotic logistic map [2,12]. The coherence manifests itself in the mutual information [2]. On the other hand the temporal correlation function similar to the Edwards-Anderson order parameter for the spin glass [14] decays to zero exponentially. Thus it may not be due to freezing between two elements [2].

All these are important observations for the turbulent regime of GCML. But this is not the whole story. Especially one should not simply conclude by the above list that the turbulent regime of GCML (and also EGCML) is a regime with complete randomness at small N and with the hidden coherence for larger N. The MSD and distributions previously reported [2] are only for the limited regions of the turbulent regime where the mean field distributions looks semi-gaussian and the violation of LLN for large N is remarkable. But

there do exist regions in the turbulent regime where the coherence is suppressed strongly and the MSD obeys LLN in a good approximation. Oppositely there are also large regions where the final attractors are two or three clusters which evolve stably (until the end of 10^6 iterations) in period three; a grand periodicity in the turbulent regime. Furthermore even in a large part of the 'hidden coherence' region the distribution is not really gaussian; it is only semi-gaussian (trapezoidal) or has visible peaks on top of semi-gaussian distribution. We can detect the remains of the periodic coherent motion by an analysis of the decay of a temporal correlation function for these regions. The turbulent regime is actually the region which is full of periodicity remnants and the hidden coherence is realized in between the genuinely turbulent regions and manifestly periodic regions. The EGCML shares the same features with GCML. In the following we show these facts by an extensive analysis over the whole turbulent regime.

A. An extensive statistical analysis of the turbulent regime of GCML and EGCML

We measure the distribution of h_n and its MSD at every point on the grid on the $N-\varepsilon$ plane in the turbulent regime at a fixed value of the nonlinear parameter a. Here we choose $a = 1.9$ as a canonical value but our observations below generally hold for other values of a larger than 1.6. At $a = 1.90$ the turbulent regime is from $\varepsilon = 0$ to 0.15 for GCML and from $\varepsilon = 0$ to 0.12 for EGCML (see Fig. 1 a and b). Thus we set a 25×61 $N-\varepsilon$ grid where the lattice size $N \equiv k^2$ varies from $k = 3$ to 51 with an increment of k two[6] and the coupling ε varies from 0 to 0.12 with an increment 0.002. At every point on the $N-\varepsilon$ grid with a fixed at 1.90, the maps are iterated from a random start and the mean field h_n is measured during the time interval between $n = 10^4$ and 10^5. Thus the result for one run at $a = 1.90$ is a 25×61 table of distributions and each distribution is a histogram of 9×10^4 h_n. We

[6]This increment of N is necessary for two-dimensional EGCML with the periodic boundary condition. For GCML we keep the increment the same for the sake of comparison.

have repeated the run several times for the same a and verified that the general result is independent from the change of the initial configuration of randomly produced maps.

We have also checked in two ways that our $N-\varepsilon$ grid is sufficiently fine to see the general feature of the turbulent regime. Firstly we randomly chose more than a hundred squares of the grid and subdivided them. Using this finer grid we have verified that either the variation of ε or N within each square does not cause any significant change of the distribution (a local check). Secondly the compiled $1525(= 25 \times 61)$ distributions are sufficient to make an animated show of the distribution. We observed by this animation that the distribution changes systematically the shape with variation of either ε or N over the whole $N - \varepsilon$ grid though the onset of the apparent periodic distribution is quite rapid (a global check). We find that a special care must be taken over for the transient time when we are on the edge of the periodic window region. There the maps may fall sometimes into the final periodic attractor after, for instance, 8×10^4 iterations but sometimes only after 10^2 iterations depending on the random initial values. For this edge region we have done a separate analysis using a sequence of runs, each consists of 10^5 to 10^6 iterations. We comment on this region in Sec. V D. This simple but tedious analysis[7] was the start of the work to unveil the real feature of the turbulent regime.

B. The MSD surface

In Fig. 8a and b we show the MSD of the mean field (h_n) distributions at $a = 1.9$ as a surface plot over the $\varepsilon - N$ grid for GCML and EGCML respectively. Both MSD and N are plotted in the logarithmic scale so that the linear edge of the surface in the front panel at $\varepsilon = 0$ is of course due to LLN. For a non-zero but very small ε (≤ 0.01), the LLN still holds

[7] A GCML run can be done by a personal computer with a Pentium 300MHZ CPU in a day but for EGCML we used a hundred PCs(Pentium 90MHZ) simultaneously for a week during Christmas in 1996. Then we assigned ranks of 1525 distributions for both models.

to a good approximation but for a larger ε we can clearly see that the surfaces have many peaks. The global features of the MSD surfaces may be summarized as follows.

The valleys : At the valleys of the surface the MSD still approximately respects LLN and we may call these valleys as genuinely turbulent regions.

Apart from the valleys LLN does not hold. This does not imply the real violation of the LLN in the ensemble average [12]. What is meant by the violation of LLN here is that there is a larger fluctuation in the time series of h_n than expected by LLN. We are interested in detecting the coherence among the evolving elements by the enhanced MSD. For both GCML and EGCML the peaks divide into two classes except that the peaks are more parallel each other for GCML. Below we quote figures for GCML.

The first-class peaks : We can see two very high and broad peaks at $\varepsilon \in 0.032 - 0.034$ and $\varepsilon \in 0.042 - 0.054$ and LLN is violated extremely on them. Here the excess MSD is observed also for small N. Let us call them as the first-class peaks of the MSD surface.

The second-class peaks : Separated by the large first-class peaks there are also several minor peaks. Their locations for $a = 1.90$ are

$$\varepsilon \approx 0.012, 0.016, 0.020, 0.024 \tag{5.2}$$

$$\varepsilon \approx 0.062, 0.07, 0.074, 0.08, 0.088 - 0.098, 0.106 - 0.108 \cdots$$

Let us call them as the second-class peaks. Provided that one keeps eyes only on the second-class peaks the MSD first decreases with increasing N following LLN and then above certain threshold N_δ the MSD ceases to decrease and remains approximately in a plateau. This is a characteristic behavior of MSD at the hidden coherence. However we show below that the h_n distribution is not a gaussian but is a distorted gaussian in the bulk of the second-class peak regions.

C. The mean field distributions

Now we analyze directly the table of 25×61 distributions of the mean field h_n at $a = 1.90$ for both GCML and EGCML to understand how the distribution looks like for the

enhanced MSD regions. Before this analysis we had thought from the literature [2] that the distributions are all gaussian with possible MSD enhancement at least for the central region of the h_n histogram [8]. But to our first surprise we find that there are a variety of distributions involved in the table of GCML and EGCML.

We assign each distribution a pattern classification number or a rank from zero to four by its shape.

0: The distribution is gaussian. Compared with the gaussian distribution at $\varepsilon = 0$ with common a and N, the MSD agrees within 20 percent error.

1: Still gaussian but with more than 20 percent increase of the MSD. At large N we see the MSD can become even more than twice.

2: A singly peaked distribution but the shape is distorted from gaussian. Typically a gaussian-like peak polarized to the right or left, or trapezoidal.

3: Either it has a few sharp peaks on top of a broad band, or it is an apparent overlapping gaussian distribution. It manifestly shows the periodic motion of elements.

4: The distribution consists of a few sharp peaks only.

At rank zero the mean field distribution obeys both LLN and CLT and the maps may be thought as independent random numbers with a common probability distribution. Oppo-

[8] Since the h_n distribution is limited in the range $[-x_L, x_L]$, it cannot be a finite width gaussian distribution over $(-\infty, \infty)$. When we discuss whether the h_n distribution is gaussian or not we concern whether the essence of the CLT, that the convolution of independent random distributions peaks like gaussian in the central region, is in action or not. The ratio of the fourth to the second moment must be three for a perfect gaussian and for the h_n distribution a small deviation from three is reported [2]. But it is sensitive to the tail region and the dynamics in the central region is obscured in a ratio. For instance, the rank three distribution below is often two overlapping gaussian peaks due to the periodic clusters with high mixing but a ratio of moments cannot tell it.

sitely at rank four the maps are in periodic motion and so is the mean field. The ranks are organized in a way that the periodicity of the elements becomes more manifest with an increase of the rank.

In Fig. 9a and b we show the rank distribution on the $N - \varepsilon$ grid as a density plot for GCML and EGCML respectively. We find the followings.

(1) There is a remarkable match between the MSD surface plots and the distribution density plots[9]. The MSD surface is high (low) wherever the rank of the distribution is high (low). The rank distribution plot is almost a contour plot of the MSD surface. This is highly non-trivial. That the rank plot is a contour plot of a surface means that there occurs no jump of ranks when we vary either ε or N. For instance to go to rank four from rank zero one has to pass the intermediate rank regions. This indicates that the dynamics of maps changes continuously (not necessarily smoothly) when either ε or N is varied over the turbulent regime.

(2) The fist class peaks of the MSD surface occur just at the rank three and four distributions. The first-class peaks are due to the periodic coherent motions of elements.

(3) In the second-class peaks the mean field distribution is rank zero (both CLT and LLN hold.) for small N. When N is increased with ε fixed, it becomes rank one (CLT holds but LLN violated) above certain threshold. With a further increase of N it almost always become rank two (even CLT is not fully operative). No higher rank distribution (rank three or four) appears in the second-class peak regions. Only in small band(s) of ε (for instance, only in a narrow band around $\varepsilon = 0.07$ for $a = 1.90$) the rank remains one for large N.

(4) The threshold between rank zero and rank one distribution precisely agrees with the break point N_δ of the drop of MSD following LLN. For reference we superpose the approximate curve for the N_δ ($N_\delta \propto 1/\varepsilon^2$) given by [2] in Fig. 9 and indeed it runs roughly

[9] In order to make a 'blind test' we never compared the ranks with the MSD surface before we finish the whole task of rank assignment.

between the rank zero and rank one regions. We consider the fact in (3) that the rank one distribution changes smoothly to the rank two distribution with increasing N is a key to the hidden coherence; it indicates that the coherence between maps 'hidden' in the rank one distribution region becomes manifest in the adjacent rank two distribution region.

Hereafter we focus our attention to GCML. In Fig. 10 we show a sample of (3) in the left three boxes. We fix a and ε ($a = 1.90, \varepsilon = 0.08$) and give the h_n distributions at various N ($N = 30,\ 100,\ 3000$) which are sampled in 10^5 iterations from random starts discarding the first 10^4 steps. We also display in each box the h_n distribution with ε set to zero as a reference distribution. In the box for $N = 30$ the two distributions are indistinguishable. The h_n distribution is hence rank zero and both LLN and CLT hold. At $N = 100$ the distribution with $\varepsilon = 0.08$ becomes a gaussian with enhanced MSD. It is rank one and indicates the 'hidden' coherence; CLT holds but LLN does not[10]. Now in the third box at $N = 3000$ the distribution turns out to be the rank two distorted gaussian distribution. Even CLT no longer holds. In the fourth box we also exhibit the h_n distribution at $a = 1.99$, $\varepsilon = 0.08$ and $N = 1000$. This is in our classification the rank three distribution with two overlapping gaussian peaks. In the model with $a = 1.90$, we can move to this dynamics region by varying ε, i.e. by traversing the turbulent regime. This point is further substantiated in the following subsections.

At this point we need some explanation on the terminology of the *hidden* coherence. The interesting phenomenon that above some N_δ the LLN in the time series is violated certainly occurs but now we have found that it is restricted to the second-class peak regions only. There are valleys where LLN approximately holds even for large N and also the first-class peak regions where LLN is violated even for small N. And now even in the second-class peak

[10] A figure corresponding to these two boxes was given in Fig.1 of ref. [2] (At $a = 1.99$ and $\varepsilon = 0.1$). But the continuous change of dynamics to higher ranks, such as from the second box to the third box was not noted.

regions the place where the CLT holds (with LLN violated) is again restricted. For $a = 1.90$ it is only a narrow band around $\varepsilon = 0.07$ and it moves to the larger ε for larger a. Thus if a distinction between the rank one and two distribution is made and the hidden coherence is defined strictly as the phenomenon that CLT holds with no approximation (i.e. excluding the rank two distribution) but with broken LLN, it can live only in a very restricted region among the second-class peak regions. We will further show below that a careful analysis of the decay exponent of the temporal correlator can also unveil the coherence among maps.

But still we consider the first discovery [1] of the onset of the violation of LLN *even in the region where the CLT holds (rank one)* is remarkable. Our point in emphasizing the distinction between rank one and two distributions is that the recognition that the rank one dynamics region is adjacent in the $N - \varepsilon$ space to the rank two dynamics region which in turn is adjacent to the rank three and so on enables us to track down the change of dynamics and thus leads us to a working hypothesis that the hidden coherence is the most modest manifestation of the coherent quasi-periodic motion of maps ubiquitous in the turbulent regime.

D. Traversing the GCML turbulent regime

Now that we have identified the various regions in the turbulent regime with distinct manifestation of periodicity let us to proceed to clarify how the dynamics of maps in these regions are related each other. To collect necessary information it is best to traverse the turbulence regime at fixed a, N and varying ε as a tuning parameter. In Fig. 11 we present a sample record of such an expedition at $a = 1.90, N = 1000$. The first column shows the mean field distributions as well as the single map distributions. The former is the average during the steps from $n = 10^4$ to $n = 10^5$, and the latter is the average during the last 2×10^3 steps of 10^5 iterations. In the second column the rank of the h_n distribution is denoted at the top in each box. The evolution of a hundred selected maps is displayed for the last seven steps. In order to chase the periodic motion of elements we devise a simple

temporal correlator of the *relative coordinate vector* $\tilde{\boldsymbol{x}}(n) \equiv (x_1(n) - h_n, \cdots, x_N(n) - h_n)$ of maps around the mean field:

$$C(t) = \left\langle \frac{\tilde{\boldsymbol{x}}(n+t) \cdot \tilde{\boldsymbol{x}}(n)}{|\tilde{\boldsymbol{x}}(n+t)||\tilde{\boldsymbol{x}}(n)|} \right\rangle. \tag{5.3}$$

The average over n is taken for the last 10^3 steps. This correlator is displayed in the third column. We show it just as defined by (5.3) but for the measurement of the decay exponent we quote values obtained by the signed logarithm plot ($f(x) \equiv (x/|x|)\log(|x|)$) of $C(t)$. For smaller lattice analysis we also averaged over data with different initial configurations to improve the statistics but this did not cause any significant change for the exponent estimation. The last column shows the return maps of h_n (the set of points (h_n, h_{n+1})) from the last 10^3 steps.

Let us start at pure randomness $\varepsilon = 0$. The map average distribution has many sharp peaks with fractal hierarchy structure reflecting the unstable fixed points of a single map in the chaotic region. The h_n distribution obeys of course both LLN and CLT and naturally sharp gaussian (rank zero) for $N = 1000$. The evolution plot shows a simple logistic pattern and the return map is a simple tiny cloud of points. The correlator is one at $t = 0$ by definition and decays almost instantly.

We can foresee that periodicity three window in the first-class peaks is waiting us ($\varepsilon \in [0.032, 0.054]$) but let us choose $\varepsilon = 0.028$ to see if any precursor of it emerges. We find that the h_n distribution has become rank one. The map average distribution has lost some sub-peaks since any one of the maps is pulled by the mean field in fluctuation and it has become more difficult for it to stay at the unstable sub-fixed points for long time. The coherence is still invisible neither in the map evolution nor in the return map. But we find that remarkably the correlator now oscillates in period three and decays exponentially (≈ 30 steps for 10^{-3} decay). This period three damping oscillation of the correlator starts at $\varepsilon \approx 0.02$ except for the valleys and the decay exponent becomes smaller for larger ε.

At $\varepsilon = 0.030$ the h_n distribution is rank two. We are now very close to the first-class peaks. The correlator survives longer period (≈ 70 steps for 10^{-3} decay) in period three

motion. But the return map does not sense this. From the evolution diagram we can immediately tell that this failure of the return map is due to mixing of the maps between the quasi-clusters at a high rate. This inadequacy of a return map should be noted.

At $\varepsilon = 0.032$ we are on the edge of the first-class peak regions. Now very careful analysis is necessary to account for the first transient behavior of the maps. The truncation of the first 10^4 steps is not sufficient and we have to watch the evolution carefully until at least during 10^5 steps. We show two typical samples at $\varepsilon = 0.032$.

In the first sample at $\varepsilon = 0.032$ the maps remain in a few quasi-clusters with mixing until the end of the run. The unstable quasi-clusters oscillate in period three and the correlator decays to 10^{-3} only after $t \approx 140$ due to the smaller mixing than before. Now we can see in the return map three clouds of points turn out. The map average distribution has only three prominent peaks and all other sub peaks are lost. The corresponding h_n distribution is rank three with both a visible peak and a shoulder on top of a broad band. The high MSD of the h_n distribution comes from the large separations between the dominant unstable fixed points of the maps in interaction. This distribution is an example of overlapping gaussian distributions. For the perfect periodic motion of the tight clusters, sharp delta peaks would be observed in both map and h_n distributions. Due to the decay of the quasi-clusters caused by the mixing the sharp delta peaks become broad and turn into overlapping gaussian distributions. We frequently observed more prominent overlapping two or three gaussian peaks in the whole analysis of the turbulent regime using both a and ε as tuning parameters. (See, for instance, the fourth box in Fig. 10.) In the second sample at $\varepsilon = 0.032$ the maps literally dropped into period three attractor of three clusters at $n \approx 8 \times 10^4$. As the map evolution plot shows the map positions in each cluster exhibit some variance in evolution so that we would better describe the clusters as quasi-clusters. The broad band in this rank three h_n distribution is an artifact of the transient motion before the maps fall into the final attractor. There is no mixing at all between the clusters. The h_n distribution is a sharp single peak and the h_n return map is confined in a very small range. This is due to the fact that the three clusters happen to be almost equally populated in this run so that the mean

field fluctuation is minimized.

At $\varepsilon = 0.042$ we are at the summit of the first-class peak. Here the maps almost always drop into period three attractor of two clusters. By only two clusters in period three motion the mean field must also fluctuates in period three. Thus the h_n distribution has sharp three peaks and MSD turns out high. The value of MSD is solely determined by the dynamics of clusters and N independent. Also the return map is widely spread.

While we traverse the summit of the first-class peaks till $\varepsilon \approx 0.52$ the attractor remains in period three. Sometimes it bifurcates to period six.

In further expedition we depart from the first-class peaks and go down into the second class peak regions. Everything then occurs in reverse way in this descent till $\varepsilon \approx 0.058$.

From $\varepsilon \approx 0.06 - 0.1$ we traverse the second-class peaks as well as the valleys. At the second-class peaks the correlator survives above 10^{-3} until $t \approx 30 - 40$ but with no apparent low periodicity. Then above $\varepsilon \approx 0.10$ the correlator starts again catching the precursor of the period two opposite phase motion in the two-cluster regime of the GCML. Thus the indeterminacy of the period of quasi-clusters beyond second peak regions comes from the fact that the regions are just in between the period three window and two-cluster opposite-phase motion regions. After $\varepsilon \approx 0.1$ the correlator shows perfect period two motion and the decay is smoothly prolonged with increasing ε. At $\varepsilon \approx 0.15$ it only decreases by a few percent even at $t = 500$. Correspondingly, above $\varepsilon \approx 0.1$ the middle peak in the map average distribution starts approaching to the peak at higher x and above $\varepsilon \approx 0.13$ the map average distribution splits into two (no events in the middle gap region). Still in the evolution plot we can see the maps are in loose clusters with mixing between each other. The high MSD of the rank two and three distributions above $\varepsilon \approx 0.1$ is clearly induced by the widely spread dominant unstable fixed points of low periodicity.

E. The dynamics in the turbulent regime

We have done a similar analysis at various a up to $a = 1.99$ and verified that all above features at $a = 1.90$ are unchanged. The various manifestation of the periodicity is summarized in Table I for $a = 1.90$. Only a minor difference for larger a is that the regions of rank one distribution above the first rank MSD peaks become larger shifted to larger ε and also the rank three distribution starts to appear there. Since the rate of the mixing of maps between clusters is the key to the turbulent regime we have also measured the temporal correlator of the clustering pattern matrix similar to the Anderson-Edwards order parameter [2]. It exhibits the same variation of the decay exponents with our correlator. We examine below how the dynamics in various regions are related each other.

(1) Let us first compare the dynamics of the periodic regions with that at $\varepsilon \approx 0$. At $\varepsilon \approx 0$ maps evolve almost independently with long visit at all of the unstable fixed points of the logistic map. Thus the map average distribution has many peaks with fractal structure peaking. Since the maps behave as almost independent random variables with the same probability distribution, naturally both LLN and CLT hold. At the periodic window in the first-class MSD peak regions, on the other hand, the $1 - \varepsilon$ focusing effect tunes the maps to form tightly bound two or three clusters mutually oscillating in period three attractor and this leads to the rank four distribution with sharp delta peaks. The dynamics of clusters in the periodic attractor is solely determined by a, ε and the effective couplings between the clusters determined by the population *ratios* among the clusters[11]. The MSD of the h_n distribution is again determined by the a, ε and the population *ratios* between the clusters, and there is no room for the explicit N dependence. Similar coherent dynamics is realized also in the ordered two-cluster regime beyond the turbulent regime ($\varepsilon > 0.2$ for $a = 1.90$). The turbulent regime has a period three window in the center of it and the two-cluster

[11] We have numerically checked that the matrix-coupled three-map model similar to (4.3) does exhibit the same period three attractor at the same value of ε.

regime beyond it. We discuss below how these affect other regions.

(2) When ε deviates from the range necessary for the period three cluster dynamics (or for the period two-cluster dynamics), the perfect synchronization of maps among each cluster is no longer realized. But what we observed in the last subsection is that even for some large deviation of ε the maps still move under certain coherence if N is beyond the threshold N_δ. Such coherent motion of maps can be best described by *unstable quasi-clusters* the decay life of which is given by the inverse of the exponent of the correlator. The maps now divide into a few masses *at any instance* of the evolution. In a short time scale these masses oscillate mutually in the same periodicity as before as we observed in both the map evolution plot and the correlator[12]. But the variance of map positions among each mass is not so small and the synchronization of maps in each mass is also not perfect. Hence we call these masses as quasi-clusters. Due to the fail of perfect synchronization, the quasi-clusters mix each other by the exchange of maps and soon they loose their identities. So the quasi-clusters are unstable and have short life time. But still at any instance of evolution there do exist quasi-clusters. The quasi-clusters defined at a certain time decay but in the evolution of maps new quasi-clusters are kept created. We may regard these quasi-clusters as *remnants* of the perfect periodic motion of maps. In fact when we approach the periodic regions the decay exponent of the correlator decreases smoothly, that is, the life time of the quasi-clusters increases smoothly, signaling the phase transition from turbulence to periodicity.

In pure turbulence the system is invariant under the exchange of maps, while in the system of maps divided into clusters this permutation symmetry is broken. Simultaneously the system in pure turbulence is invariant under the temporal translation, while the system in periodic motion is only invariant under the temporal translation just for the period. The self-organized state of maps in periodic quasi-clusters emerges as the state of broken symmetry from pure turbulence by a weak self-coupling and it emerges only for large N.

---

[12] Note that the quasi-clusters are hardly seen in the return map analysis because of the mixing.

This is interestingly reminiscent of the onset of ordered parameter at the spontaneous break down of the global symmetry in the field theory where an infinite number of dynamical degree of freedom is necessary in order to support the ordered vacuum. See, for instance, Weinberg [19] where the broken symmetry state of a chair is elucidated.

It is important that the maps in the quasi-clusters approximately follow the previous cluster attractor in the life time of the quasi-clusters. This means that the h_n distribution is controlled by the scale of the previous attractor approximately and again determined by the a, ε and the population *ratios* and not by N. Thus there emerges a h_n distribution whose MSD does not decrease with N and LLN is violated. Depending on the rate of mixing and the allowed population ratios at the ε, distributions of various ranks emerge.

(3) If the deviation of ε from the necessary range for periodic cluster attractor is not large, the failure in the map synchronization is not also large. The quasi-clusters decay by low rate mixing of members so the correlator survives for long time exhibiting clearly the periodicity of the previous periodic cluster attractor. But the would-be delta-peaks of both the average map distribution and the h_n distribution at no mixing now change into overlapping gaussian distributions with visible separation between the peaks. These changes of the correlator and the h_n distribution at small deviation of ε are precisely what we observe around the first-class MSD peaks and near the upper boundary of the turbulent regime adjacent to the ordered two-cluster phase.

With further deviation of ε the mixing rate becomes higher. The correlator decays more quickly and the h_n distribution becomes from rank three to rank two - the distorted gaussian distribution. We observe this when we go down from the first-class peaks to the region of $\varepsilon \approx 0$ or when we approach the first-class peak regions from above. In the former case the correlator keeps exhibiting the period three damped oscillation even if we go down into the rank one h_n distribution region. In the latter case the periodicity of the correlator becomes indefinite below $\varepsilon \approx 0.1$ for $a = 1.90$ since naturally we are coming down from two-cluster regime with period two to the period three window, and we finally loose the track of a periodicity remnant (rank two distribution) when we go further into the narrow band of

rank one h_n distribution region. This is the genuine hidden coherence region.

(4) The place the hidden coherence can live has now become very limited since we have improved the sensitivity to the coherence effect. In the old analysis [2], the distinction between rank one and two distributions was ignored and neither the change of the decay exponent of the correlator with ε nor the periodicity of it was analyzed. The periodic window and the valleys were not discussed also. Then the coherence seemed to live hidden everywhere in the turbulent regime if $N > N_{th}$. Now, both the periodic window with manifest coherence and the valleys with valid LLN should be excluded first of all. Furthermore, in the regions where the correlator has clearly caught the periodicity remnant, it is no longer legitimate to describe the coherence as hidden. Thus, regarding the correlator the coherence is hidden only in a limited region in between the period-three and period-two remnant regions among the second-class MSD peak regions. This is the region with $\varepsilon \approx 0.06 - 0.1$ for $a = 1.90$. See Table I and Eq. (5.2). Here the correlator does show longer decay time (10^{-3} decay within $20 - 40$ steps) than that at $\varepsilon \approx 0$ but it decays with large fluctuation showing no low periodicity. This is natural for the region in between two different periodicity regions.

But not only the correlator but also the shape of the h_n distribution is a vital quantity to keep track of the change the dynamics. Almost everywhere in the possible residence of the hidden coherence regarding the correlator, the h_n distribution is rank two (rather than gaussian) and naturally understood as the smooth continuation of the rank three overlapping gaussian distribution. The CLT is apparently violated here and the distribution is still controlled by the scale of the attractor.

Therefore, the place where the coherence is literally hidden from both the correlator and distribution analyses is now very limited. It is the narrow band at $\varepsilon \approx 0.07$ for $a = 1.90$ and around $\varepsilon \approx 0.09 - 0.11$ for $a = 1.99$ where the h_n distribution is really gaussian with enhanced MSD (rank one) and the correlator does not show the low periodicity. Here the coherence seen in the enhanced MSD can be only substantiated either by the finite mutual information or by the instability of the FP fixed point distribution. But in (3) above we successfully tracked down the smooth change of distribution (and the corresponding change

of the decay exponent of the correlator) with the deviation of ε from rank four down to rank two distribution regions which surround the literally hidden coherence region. This gives a new way to look at the hidden coherence. Higher rate mixing with further smooth deviation of ε should necessarily weaken the coherence among the maps and change the distorted gaussian (rank two) to the gaussian distribution. If the scale of the attractor still remains to govern the map dynamics the h_n distribution with N-independent MSD would emerges. We propose this last statement as a working hypothesis for the origin of the hidden coherence.

F. An Analytic Approach

Up to this point we have heavily depended on the numerical simulation. Our concern is the statistical properties of the large-size GCML (EGCML) and the Monte-Carlo simulation is naturally the basic approach to the phenomenology of such system. We have shown that a faithful extensive analysis of the data unveils amazing new features of the system. But, of course, if by some analytical method, one could relate the systematic manifestation of periodicity in the turbulent regime to the periodic behavior of the element of the system, namely the period three window of a single logistic map, it would be certainly a step forward to the real understanding of the turbulent regime. In this last subsection we discuss such an analytic approach.

Let us consider a typical case where the N maps are divided into equally populated three clusters A, B, C ($N_A = N_B = N_C = N/3$) and the clusters move cyclically round the three fixed positions x_1, x_2, x_3. In such a maximally symmetric and period three motion of GCML maps, $h(n)$, the meanfield of all maps at time n becomes a time-independent constant which is nothing but an equal weight average h^* of $x_i (i = 1, 2, 3)$. To see this let us first rewrite the meanfield using the invariance rule (2.7) as

$$h(n) \equiv \frac{1}{N} \sum_{i=1}^{N} f(x_i(n)) = \frac{1}{N} \sum_{i=1}^{N} x_i(n+1). \tag{5.4}$$

Then for the configuration in case the last average can be calculated as

$$\frac{1}{N}\sum_{i=1}^{N} x_i(n+1) = \frac{1}{N}\sum_{I=A,B,C} x_I(n+1) = \frac{1}{3}\sum_{i=1}^{3} x_i \equiv h^* \tag{5.5}$$

where $x_I(n)$ denotes the coordinate of the cluster I at time n. Therefore, if such a configuration is produced by the interaction between the maps via the meanfield, any one of GCML maps must be evolving by a common evolution equation

$$x_i(n+1) = (1-\varepsilon) f_a(x_i(n)) + \varepsilon h^* \quad (i = 1, \cdots, N) \tag{5.6}$$

We can cast the evolution equation (5.6) with a constant meanfield h^* and $f_a(x) = 1 - ax^2$ to a simple logistic map

$$y_i(n+1) = 1 - b\,(y_i(n))^2 \quad (i = 1, \cdots, N). \tag{5.7}$$

with a reduced coupling constant b by a linear scale transformation [20]

$$y_i(n) = \frac{x_i(n)}{1 - \varepsilon + \varepsilon h^*}. \tag{5.8}$$

The reduction rate r is given by

$$r \equiv \frac{b}{a} = (1-\varepsilon)\,(1 - \varepsilon(1-h^*))\,. \tag{5.9}$$

The period three window of the logistic map (5.7) starts at $b = 7/4 = 1.75$ by the tangent bifurcation and after the sequential bifurcation it closes at $b \approx 1.7903$ by the crisis. Therefore the reduction rate r must be for $a = 1.90$ in the range

$$0.921 \leq r \leq 0.942 \tag{5.10}$$

and at a given rate r within this range, (5.9) gives a curve of constraint on the $\varepsilon - h^*$ plane.

There is another constraint from self-consistency. Each of the maps y_i is related to the GCML maps x_i by the linear transformation (5.8) and so is the average value y^* of maps y_i to h^*:

$$y^* \equiv \frac{1}{3}\sum_{i=1}^{3} y_i = \frac{h^*}{1 - \varepsilon + \varepsilon h^*}. \tag{5.11}$$

Since y^* is simply an equal weight average of the period three stable orbits of (5.7), it can be estimated solely by the property of the logistic map without any recourse to the GCML evolution equation. For instance at the tangent bifurcation point ($b = 7/4, r = 0.921$), we have

$$f_b(f_b(f_b(y))) - y = b^6(f_b(y) - y)\left(\Pi_{i=1}^3(y - y_i)\right)^2 \tag{5.12}$$

and from matching of the coefficients we obtain $y^* = 1/(3 \cdot 2b) = 2/21$. Numerically we find that $y^* \approx 0.25$ slightly below the threshold ($r = 0.91$), drops sharply ($y^* \propto \sqrt{b_{th} - b}$) to $y^* = 2/21 = 0.095$ at the threshold ($r = 0.921$), and y^* gradually changes around 0.08 until the end of the window ($r = 0.942$). By eliminating h^* from (5.9) and (5.11) we obtain

$$\varepsilon = 1 - \frac{ry^*}{2} - \left(r(1 - y^*) + (\frac{ry^*}{2})^2\right)^{\frac{1}{2}}. \tag{5.13}$$

The estimated ε for $a = 1.90$ from (5.13) is

$$\begin{aligned}
A: &\quad \varepsilon = 0.0523 \quad \text{at} \quad (b, r, y^*) = (1.730,\ 0.910,\ 0.250) \\
B: &\quad \varepsilon = 0.0422 \quad \text{at} \quad (b, r, y^*) = (1.750,\ 0.921,\ 0.095) \\
C: &\quad \varepsilon = 0.0365 \quad \text{at} \quad (b, r, y^*) = (1.769,\ 0.931,\ 0.070) \\
D: &\quad \varepsilon = 0.0305 \quad \text{at} \quad (b, r, y^*) = (1.790,\ 0.942,\ 0.080)
\end{aligned} \tag{5.14}$$

The estimates A, B, C and D are evaluated respectively below the threshold, at the threshold, at the first bifurcation point at the middle, and at the upper edge of the period three window in the order of increasing b.

Before comparing with the simulation result we should note that a maximally symmetric configuration of equally populated three clusters in period three motion is assumed in deriving (5.13). Thus, the value of ε necessary for such a configuration should be deduced from the genuinely period three region, namely from the interval from B to C. We can predict that ε must be in the range (0.0365, 0.0422) for the formation of such a maximally symmetric GCML configuration. For such a configuration the meanfield should not fluctuate in time and it will show up as a deep valley in the GCML MSD surface. We have added two exterior

estimates in (5.14) expecting that these extensions will cover the asymmetrically populated clusters in period three motion.

Now let us compare (5.14) with the range of the period three first-class peaks found in Section V B, namely, $\varepsilon \in 0.032 - 0.034$ and $\varepsilon \in 0.042 - 0.054$.

Firstly there is a remarkable agreement between the range of peaks and the range of estimates A to D in (5.14). The whole period three window of a single logistic map shows up as the whole first-class peaks. A closer comparison with the observations in section V D gives further support for the link of the structure observed in the numerical simulation and the period three window of the logistic map.

1 We noted that in the deep valley of the MSD surface between the two first-class peaks the formation of three clusters in period three motion. The valley region $(0.034, 0.042)$ remarkably matches the above estimated range (0.0365,0.0422) for the maximally symmetric configuration.

2 We noted that in the upper first-class peak ($\varepsilon \in 0.042 - 0.054$) the maps almost always form only two clusters in period three motion. It is natural that the larger ε reduces the number of clusters from three to two. As we noted the extremely high MSD in the first-class peak is induced by the asymmetric population configuration ($N_A \approx N_B \approx N/2, N_C = 0$).

Furthermore we have verified by simulation that the first-class peak regions shift to higher ε when a is increased precisely in accord with the prediction by (5.13).

It is remarkable that the maps with high nonlinearity are driven into coherent synchronizing clusters with very small interaction parameter ε once it takes the tune up value. A lot of further effort has to be devoted to fully appreciate the implication. The analytic approach here is only a step forward to this direction. A survey of the overall relation of peak-valley structure of the MSD surface to the hierarchical windows of a single logistic map as well as the dynamical variation of the population configuration is now underway.

VI. CONCLUSION

In this article we have revisited the GCML and first resolved the puzzle of the posi-nega switch realized the two-cluster phase. The puzzle was that the maps posses the memory of the cluster to which they subject even though they pass through a transient chaotic process where many channels are open. We have proved that maps never mix across the mean field of them in the transient process. We have then analyzed the turbulent regime of GCML. To date the so-called hidden coherence has been the main target of interest in this region. We have presented our new finding that there exists a remarkable period three attractor regions in this regime. The turbulent regime locates in-between the genuinely turbulent region around $\varepsilon = 0$ and two-cluster regime of period two attractor and has this period three attractor regions in the center of it. We have shown that the remnant of the periodic coherence can be found almost everywhere in the turbulent regime by the measurement of the temporal correlator of the fluctuation of maps around the mean field and by the extensive analysis of the h_n distributions over the whole turbulent regime. The dynamics of the turbulent regime can be well described by the quasi-clusters with mixing of elements between each other. The hidden coherence may be regarded the most modest manifestation of this remnant periodicity. By an analytic approach we have shown that the prominent periodicity manifestation in the turbulent regime is caused by the period three window of a single logistic map.

A new extended globally coupled map lattice(EGCML) is constructed in which the interaction between maps decreases proportionally to the distance. EGCML at $d = 2$ has the same phase diagram with that of GCML. The bifurcation tree structure of the attractor of EGCML in the two-cluster regime is also the same with that of GCML. The maps in each EGCML cluster are phase synchronizing rather than synchronizing. The posi-nega switch between the two clusters is realized also in EGCML. In the chaotic transient process in EGCML-switch, formation of amazing spatial clusters of maps is observed. EGCML may be viable for the simulation of chaotic diffusion process. We have also shown that the tur-

bulence regime of EGCML is also not immune from periodicity just like GCML turbulent regime. As a whole this work is an exploration of order in the chaos. The posi-nega switch in GCML is realized because there occurs no mixing in the chaotic transient process. In the chaotic transient process in a EGCML-switch, interesting spatial clusters are formed. And the turbulent regime of both of GCML and EGCML is dominated by the quasi-clusters of maps in periodic motion.

ACKNOWLEDGMENTS

It is a pleasure to note the author's debt of gratitude to K. Kaneko. This work was started several years ago stimulated by the pioneering articles on GCML by him [1,2] and the compact model GCML has been an unfailing source of interest since then. The author is thankful to Fumio Masuda who worked on this subject together with the author until the last one year of completion and the nice collaboration time with him is memorized. Thanks also go to Hidehiko Shimada for many crucial suggestions, Hayato Fujigaki for his collaboration on the study of coupled flows done in parallel with this work, and Kengo Kikuchi for his unfailing effort on the analytic approach to GCML now underway. Last but not at least the author wishes to thank Wolfgang Ochs at the Max-Planck Institute for sharing his insight in this research and reading the manuscript.

This work was supported by the Faculty Collaborative Research Grant from Meiji University, Grant-in-Aids for Scientific Research from Ministry of Education, Science and Culture of Japan, and Grant for High Techniques Research from both organizations.

REFERENCES

[1] K. Kaneko, Phys. Rev. Lett. **63**, 219 (1989); K. Kaneko, Physica (Amsterdam) **41D**, 137 (1990).

[2] K. Kaneko, Phys. Rev. Lett. **65**, 1391, (1990);
K. Kaneko, Physica (Amsterdam) **55D**, 368, (1992); ibid., **D86**, 158, (1995).

[3] K. Kaneko, Physica (Amsterdam) **23D**, 436 (1986);
J. P. Crutchfield and K. Kaneko, *in Directions in Chaos*, edited by B. -L. Hao (World Scientific, Singapore, 1987).

[4] K. Kaneko, Physica **54D**, 5, (1991);
S. Sinha, D. Biswas, M. Azam, and S. V. Lawande, Phys. Rev. **A46**, 3193, 1992.

[5] L. M. Pecora and T. L. Carroll, Phys. Rev. Lett. **64**, 821 (1990);
T. L. Carroll and L. M. Pecora, Physica **67**, 126 (1993).

[6] J. M. Kowalski and G. L. Albert, Phys. Rev. **A42**, 6260 (1990).

[7] A. Maritan and J. R. Banavar, Phs. Rev. Lett. **72**, 1451 (1994).

[8] H. Fujigaki, M. Nishi and T. Shimada, Phys. Rev. **E53**, 3192, 1996.

[9] H. Fujigaki and T. Shimada, Phys. Rev. **E55**, 2426, 1997.

[10] A.S. Pikovsky, M.G. Rosenblum and J. Kurths, Europhys. Lett. **34**, 165 (1996).
M.G. Rosenblum, A.S. Pikovsky and J. Kurths, Phys. Rev. Lett. **76**,1804 (1996).

[11] E. Ott, C. Grebogi, and J. A. Yorke, Phys. Rev. Lett. **64**, 1196 (1990).

[12] A. S. Pikovsky and J. Kurths, Phys. Rev. Lett. **72**, 1644, 1994.

[13] See, for instance,
J.J. Hopfield, Proc. Natl. Acad. Sci. USA (Biophysics)**79**, 2554 (1982);
W.A. Little, Math. Biosci. **19**,101 (1974);

D. J. Amit, H. Gutfreund and H. Sompolinski, Phys. Rev. **A32**, 1007 (1985).

[14] M. Mézard, G. Parisi and M. A. Virasoro (Editors), *Spin glass theory and beyond,* , World Scientific, 1987.

[15] P. Bak, C. Tang and K. Wiesenfeld, Phys. Rev. Lett. **59**, 381 (1987)

[16] R. M. May, Nature **261**, 459 (1976)

[17] M. J. Feigenbaum, Los Alamos Science **1**, 4 (1980),
P. Cvitanović, in *Universality in chaos*, Adam Hilger, 1989.

[18] D. Ruelle, *Thermodynamic Formalism*, Addison Wesley, Reading, MA,1978;
Y. Oono and Y. Takahashi, Prog. Theor. Phys.**63**, 1804;
H. H. Hasegawa and W. C. Saphir, Phys. Rev. **A46**, 7401,1992,

[19] S. Weinberg, *The Quantum Theory of Fields*, vol.II, Cambridge University Press, 1996.

[20] G.Perez and H.A.Cerdeira, Phys. Rev. **A46**, 5469, 1992.

FIGURES

FIG. 1. (a) The phase diagram of GCML as determined by $N = 1000$ lattice with 1000 random initial configurations for each (a, ε). (b) That of EGCML. N=39×39 and typically 200 configurations for each (a, ε).

FIG. 2. Left box: The GCML two-cluster dynamics. The two clusters evolve repeating mapping (solid arrows) and interaction (dashed arrows). The mean field (a short solid bar) of maps is determined by the ratio θ and $1 - \theta$. The interaction pulls two clusters to the mean field at a rate $1 - \varepsilon$ and hence the mean field is unchanged. Right box: The period four attractor of two GCML clusters at $a = 1.98$, $\varepsilon = 0.3$. The black (white) circle nearer to the mean field is the majority (minority) cluster which involves 43 (57) percent of maps. If $n_0 =$ even (odd), the white (black) circle is named as the positive cluster with $\theta = 0.43(0.57)$.

FIG. 3. The self-organized attractors at $a = 1.98$ and $\varepsilon = 0.3$. (a) GCML : All maps $x_i(n)$, $i = 1, \cdots, 1000$ from 1000 random initial configurations are plotted at the position of the fraction of maps with $x_i(n) > x^*$ for iteration steps $n = 10000, \cdots, 10512$ (b) EGCML : $N = 51 \times 51$ maps from 4000 initial random configurations. The periodicity $T(\leq 2^6)$ of the set of maps is measured using the judgment condition $\sum_{i=1}^{N}(x_i(n+T) - x_j(n))^2 < 10^{-6}$. Maps are sampled only for the first one cycle of the period and the points with density less than one percent of the maximum are removed if they fall into a periodic attractor. Otherwise just as in GCML. The former gives the part with $\theta \in [0.39, 0.61]$ and the latter the rest. (c) The attractor of the matrix-coupled two maps sampled for $n = 10000, \cdots, 10512$ with the parameter θ varied.

FIG. 4. The transition from periodic attractors into the chaotic intermittent process. The GCML with $N = 50$ and $a = 1.90, \varepsilon = 0.3$. The threshold is $N_{th} = 20$. The two clusters oscillate oppositely in phase until time n_1. Both clusters start the grand chaotic motion at n_2, i.e. just after the minority cluster (dashed line) crosses the x^* line.

FIG. 5. The logistic map and transition from periodic to chaotic evolution. When a minority cluster is pulled down across x^* from region III to II by the majority cluster, both clusters are mapped together into region III (the left box). Then after a small contraction by interaction they are again mapped together in the same direction and the quasi-coherent grand chaotic motion starts (the right box).

FIG. 6. The GCML posi-nega switch mechanism. The iteration steps are denoted in unit of two in all figures. (a) The typical posi-nega switch in GCML ($N = 60,\ a = 1.98,\ \varepsilon = 0.3$). The attractor at even (odd) steps is shown in the upper (lower) diagram. The attractor on the whole, the even and odd iteration steps together, is precisely the same before and after the chaotic transition. The arrows point out that the posi-nega switch is a change in the count of the parity (even and odd) of iteration steps. (b) A typical posi-nega switch in GCML ($N = 50,\ a = 1.98,\ \varepsilon = 0.3$). Evolution of maps at even iteration steps is displayed as a surface plot. The posi-nega switch is seen as the total swapping between peaks and valleys of the surface via the chaotic transient process. The chaotically oscillating surface is horizontal at any instance reflecting the quasi-clustering in the transient process. (c) The same GCML switch with (b). The maps are distinguished by their mean field instead of x^*. The print-circuit pattern shows no mixing of maps across the mean field.

FIG. 7. (a) An EGCML switch with 25×25maps ($a = 1.9, \varepsilon = 0.3$) from a random start. In the upper diagram, black (gray) lines connect maps at even (odd) steps and arrows indicate the switch. Lower boxes show the snapshots of the lattice at the even iteration steps indicated by the vertical bars respectively. In the upper array positive and negative maps are distinguished by the mean field $\langle\langle x(n)\rangle\rangle$ while in the lower array by the x^*. The former exhibits the percolation formation of self-organized spatial clusters by synchronization. Between the snap-shots 4 and 8 the spatial clusters undergo posi-nega pattern switch. (b) A sample of cluster formation in the large EGCML ($N = 61 \times 61,\ a = 1.9,\ \varepsilon = 0.3$) by the distinction by the mean field. A remarkable pattern like globular nebula is seen.

FIG. 8. MSD surfaces of mean field fluctuation of (a) GCML and (b) EGCML at $a = 1.90$ over the $\varepsilon - N$ grid. The peaks reflect non-trivial coherence between maps in the turbulent regime.

FIG. 9. The rank distribution on the $N - \varepsilon$ grid at $a = 1.90$ as a gray-scale density plot. (a) GCML, (b) EGCML. The rank varies from zero(black) to rank four(white). An approximate estimation curve for the threshold N_δ ($N_\delta \propto 1/\varepsilon^2$) is superposed.

FIG. 10. The GCML h_n distribution sampled in 10^5 iterations from random start discarding the first 10^4 steps using 1000 bins. In each box the h_n distribution with the rank indicated at the corner is compared with the reference distribution at $\varepsilon = 0$. The left three boxes: $N = 30,\ 100,\ 3000$, $a = 1.90$ and $\varepsilon = 0.08$. The fourth box: $N = 1000$, $a = 1.99$, $\varepsilon = 0.08$.

FIG. 11. $N = 10^3$ GCML with $a = 1.90$. The variation of dynamics with the change of the coupling ε through the first-class MSD peak regions. All quantities in a row are measured in the same run (10^5 iterations) and the scales for each column are given in the top box at $\varepsilon = 0$. For $\varepsilon = 0.032$ two sample runs are shown; in the lower, maps fell into a three cluster attractor in period-three motion after 8×10^4 iterations; in the upper, they survived in quasi-random motion over 10^5 iterations. (a) The mean field distribution (marked as h) sampled discarding the first 10^4 transient steps and the map distribution (x) averaged over the last 2×10^3 steps. (b) Clustering pattern. The lines show the evolution of randomly selected 100 maps for the last seven steps and the black circle is the mean field of all $N = 1000$ maps. (c) Temporal correlator between the two relative-coordinate vectors of maps. Averaged over the last 10^3 steps. Below and slightly above the first-class peak regions (the periodic window) it decays exponentially exhibiting the period three motion of quasi-clusters. Approaching the periodic window the decay exponent smoothly decreases. (d) The return maps for the same period as (c). Less sensitive to the quasi-clusters. The arrows indicate the visible period three quasi-clusters.

TABLES

TABLE I. The various periodicity manifestation in the turbulent regime of GCML ($a = 1.90$ and $N = 1000$). Note that in each range of ε there are also valleys with an approximate LLN along with listed peaks with the broken LLN.

ε	region name	rank of h_n distribution[a]	correlator periodicity
$0.01 - 0.032$	the second-class peaks	$1, 2$	[3] [b]
$0.032 - 0.054$	the first-class peaks	$3, 4$	3 [c]
$0.054 - 0.06$	$\updownarrow$[e]	$1, 2$	[3] [b]
$0.06 - 0.1$	the second-class peaks	$1, 2$	[?] [d]
$0.1 - 0.15$	the second-class peaks	$1, 2$	[2] [b]

[a]rank 0: gaussian with LLN, 1: gaussian with enhanced MSD, 2: distorted gaussian with enhanced MSD, 3: visible peaks on top of a broad band, 4: sharp peaks.

[b]The correlator exponentially decays exhibiting the periodicity in the parenthesis. The dynamics can be described by unstable quasi-clusters in periodic motion.

[c]The correlator does not decay and oscillates in period three. The periodic window.

[d]The correlator decays exponentially with longer life time than that at $\varepsilon = 0$ but no low periodicity is observed.

[e]A slanting surface between the first and the second-class peaks.

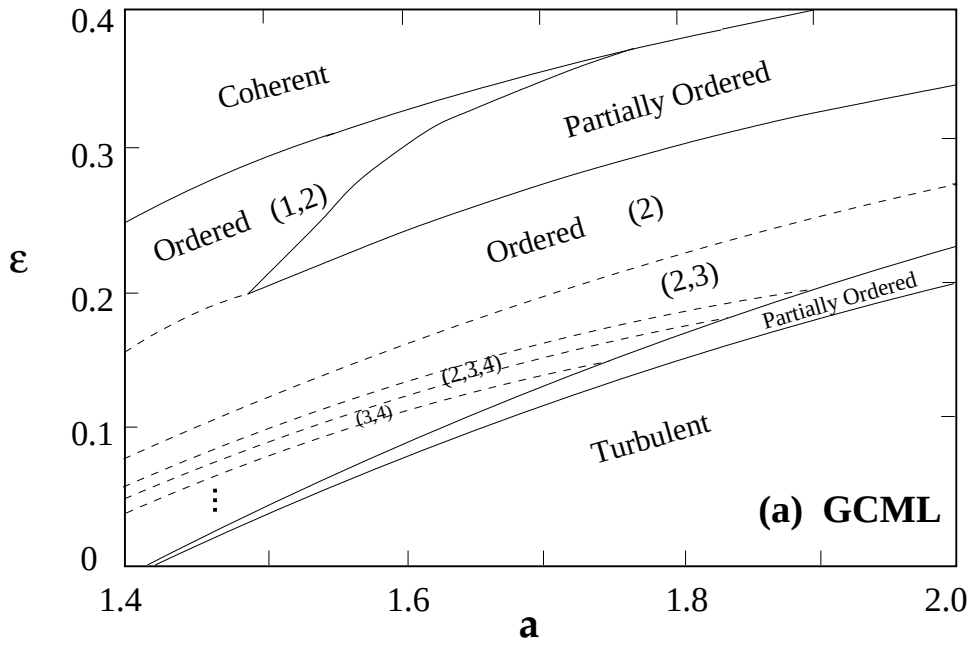
0.4
0.3
0.2
0.1
0
ε
Coherent
Partially Ordered
Ordered (1,2)
Ordered (2)
(2,3)
Partially Ordered
(2,3,4)
(3,4)
Turbulent
(a) GCML
1.4
1.6
1.8
2.0
a

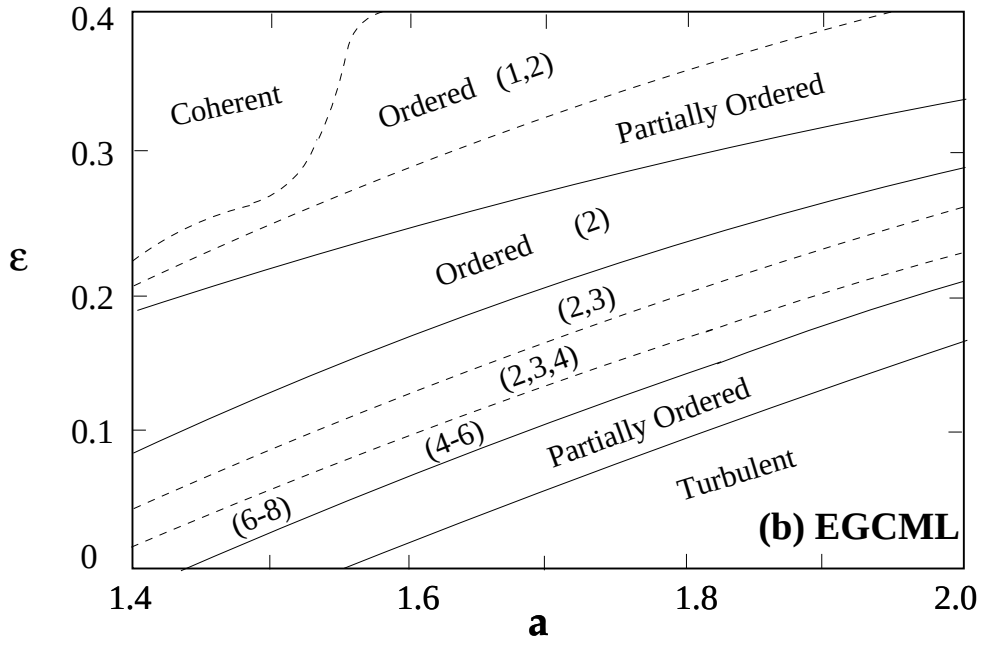
0.4
0.3
0.2
0.1
0
ε
Coherent
Ordered (1,2)
Partially Ordered
Ordered (2)
(2,3)
(2,3,4)
(4-6)
Partially Ordered
(6-8)
Turbulent
(b) EGCML
1.4
1.6
1.8
2.0
a

Fig. 1

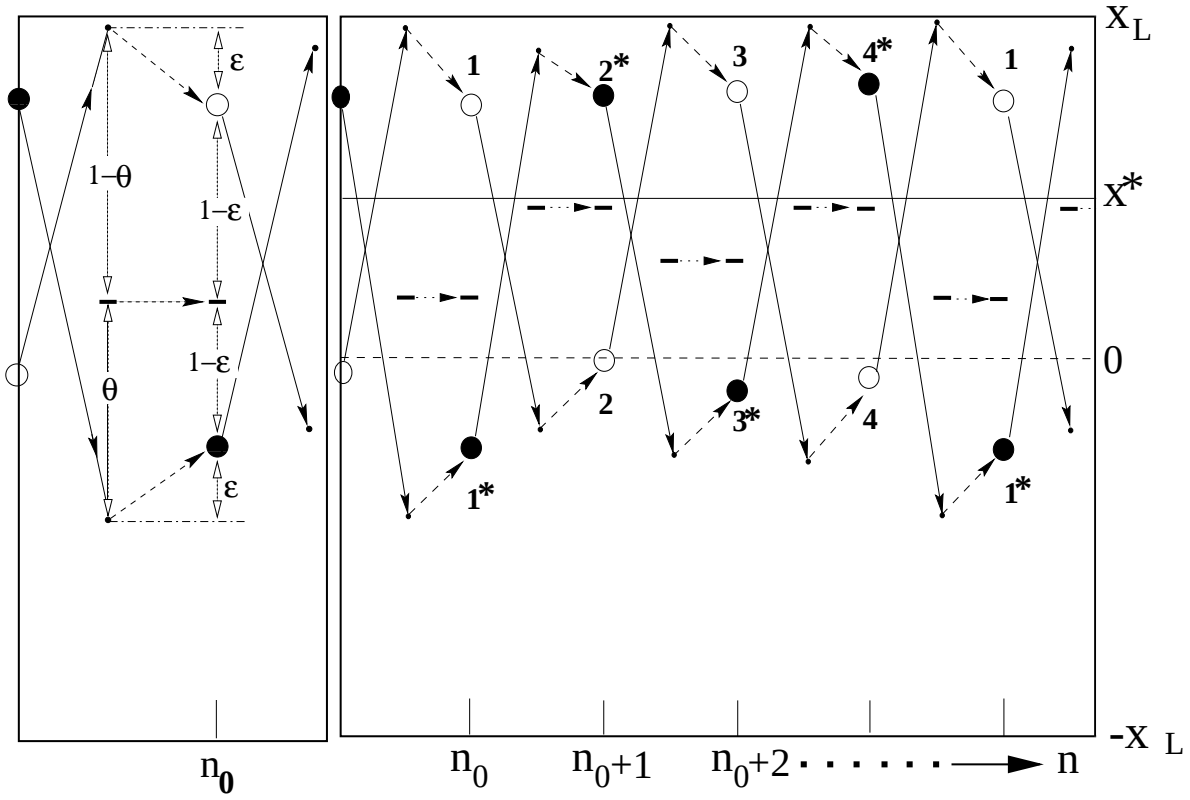

Fig. 2

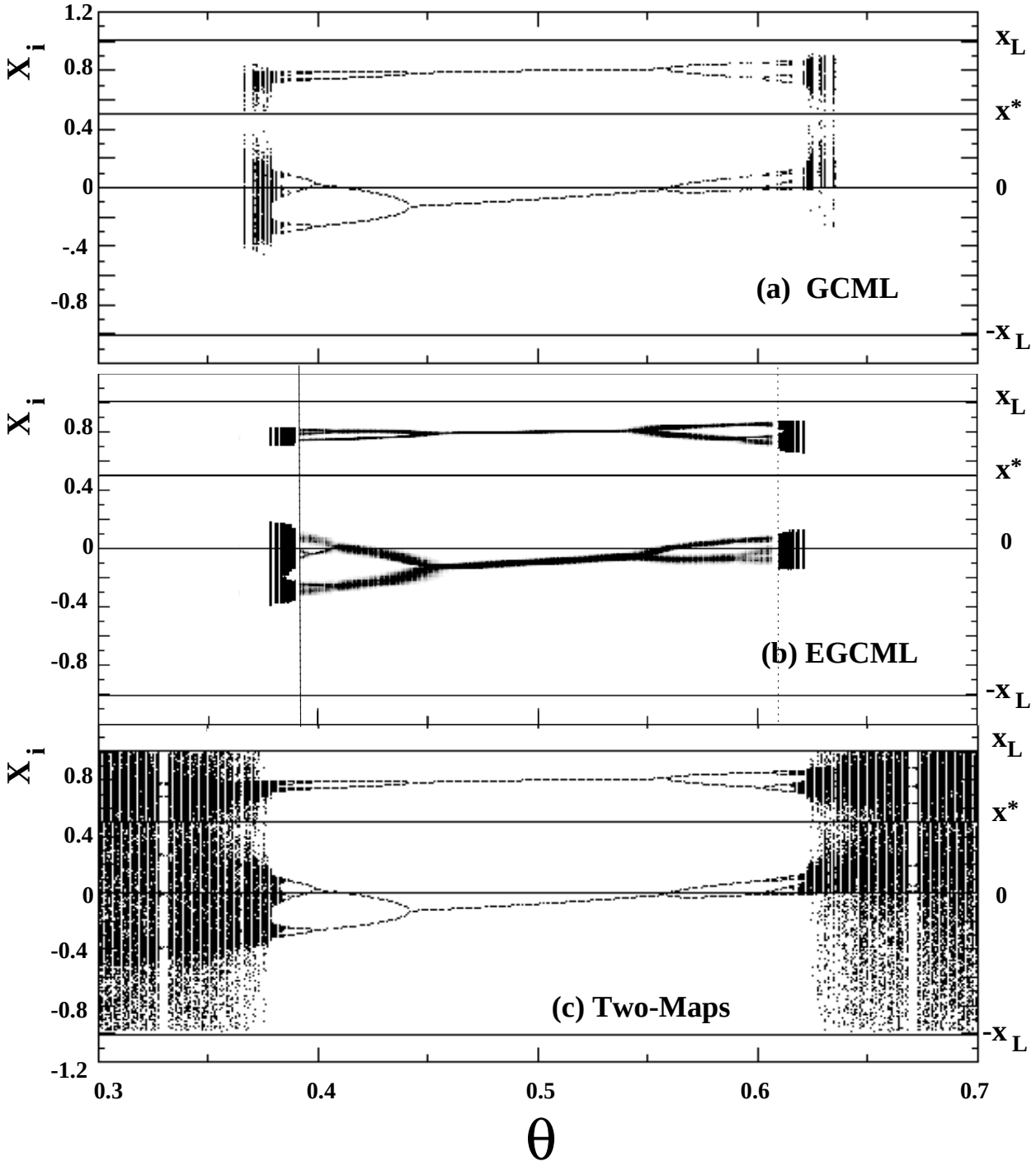
1.2
0.8
0.4
0
-.4
-0.8
X_i
x_L
x^*
0
$-x_L$
(a) GCML
(b) EGCML
(c) Two-Maps
-1.2
0.3
0.4
0.5
0.6
0.7
θ

Fig. 3

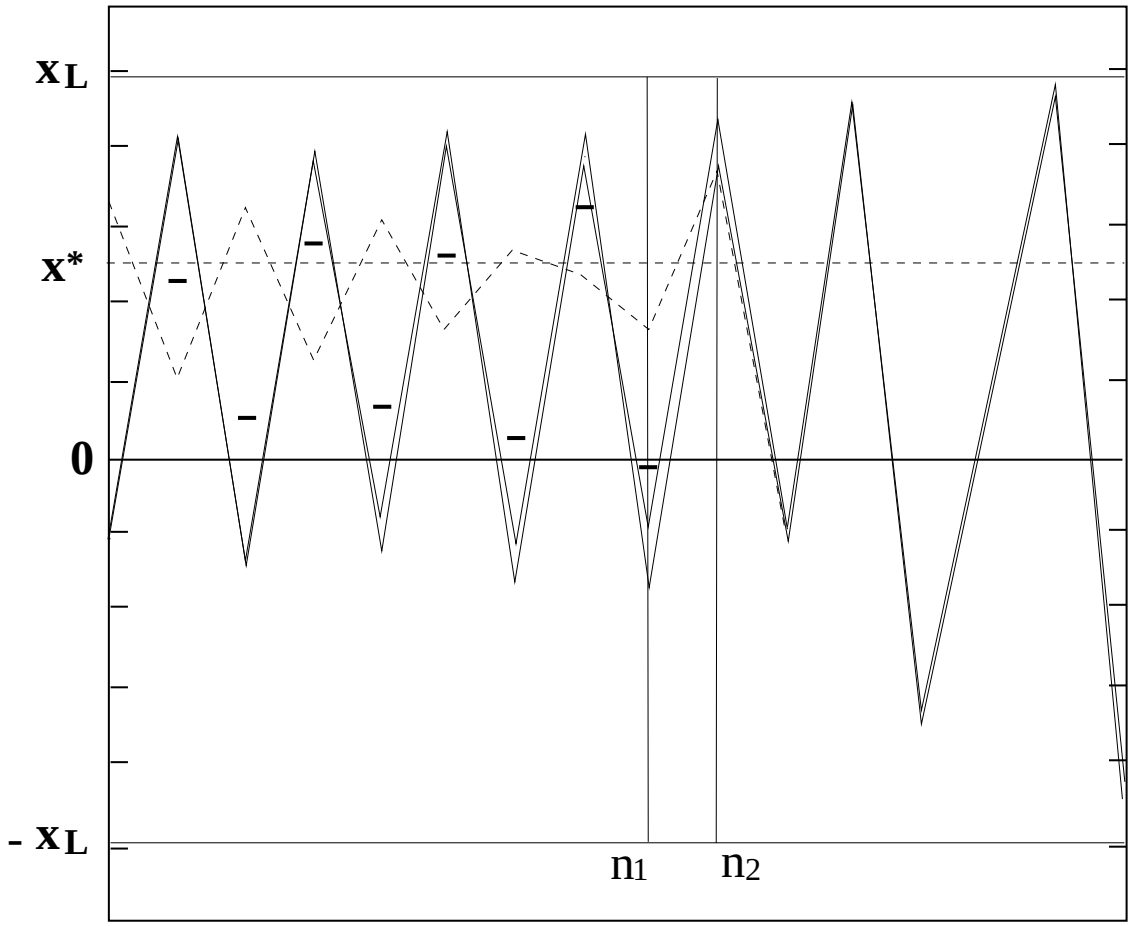

Fig. 4

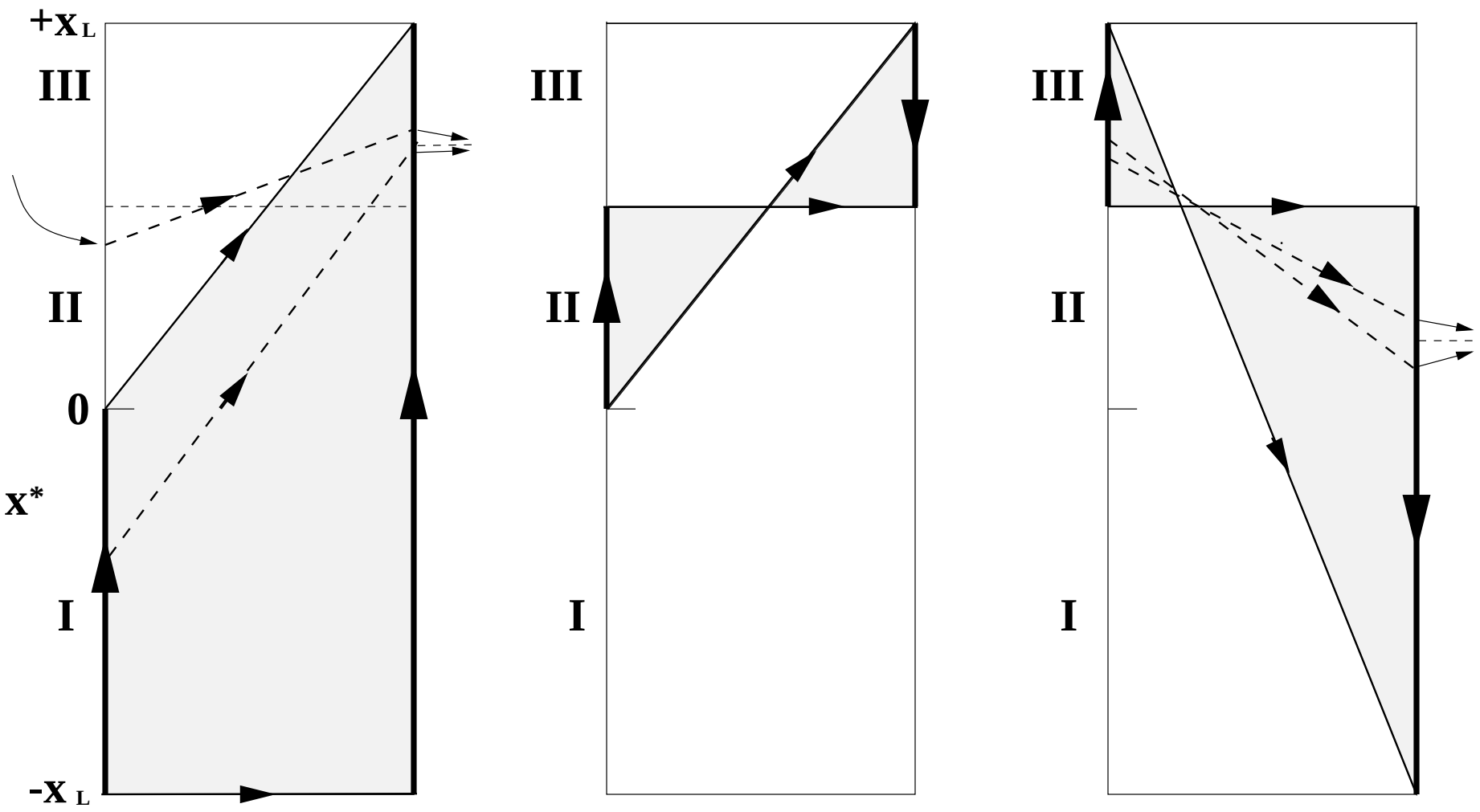

Fig. 5

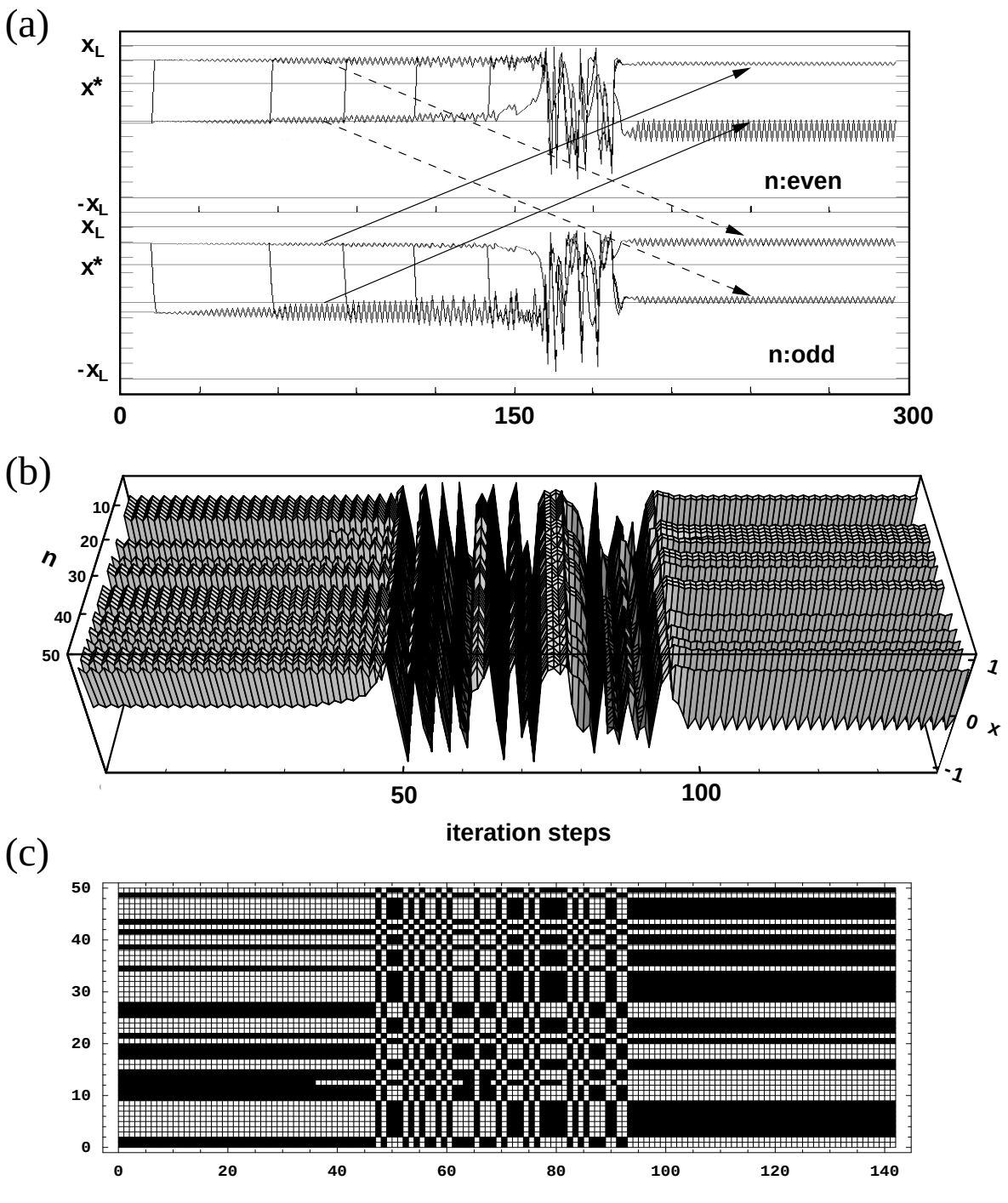
(a)
x_L
x*
$-x_L$
x_L
x*
$-x_L$
n:even
n:odd
0
150
300
(b)
n
10
20
30
40
50
1
0
x
-1
50
100
iteration steps
(c)
50
40
30
20
10
0
0
20
40
60
80
100
120
140

Fig.6

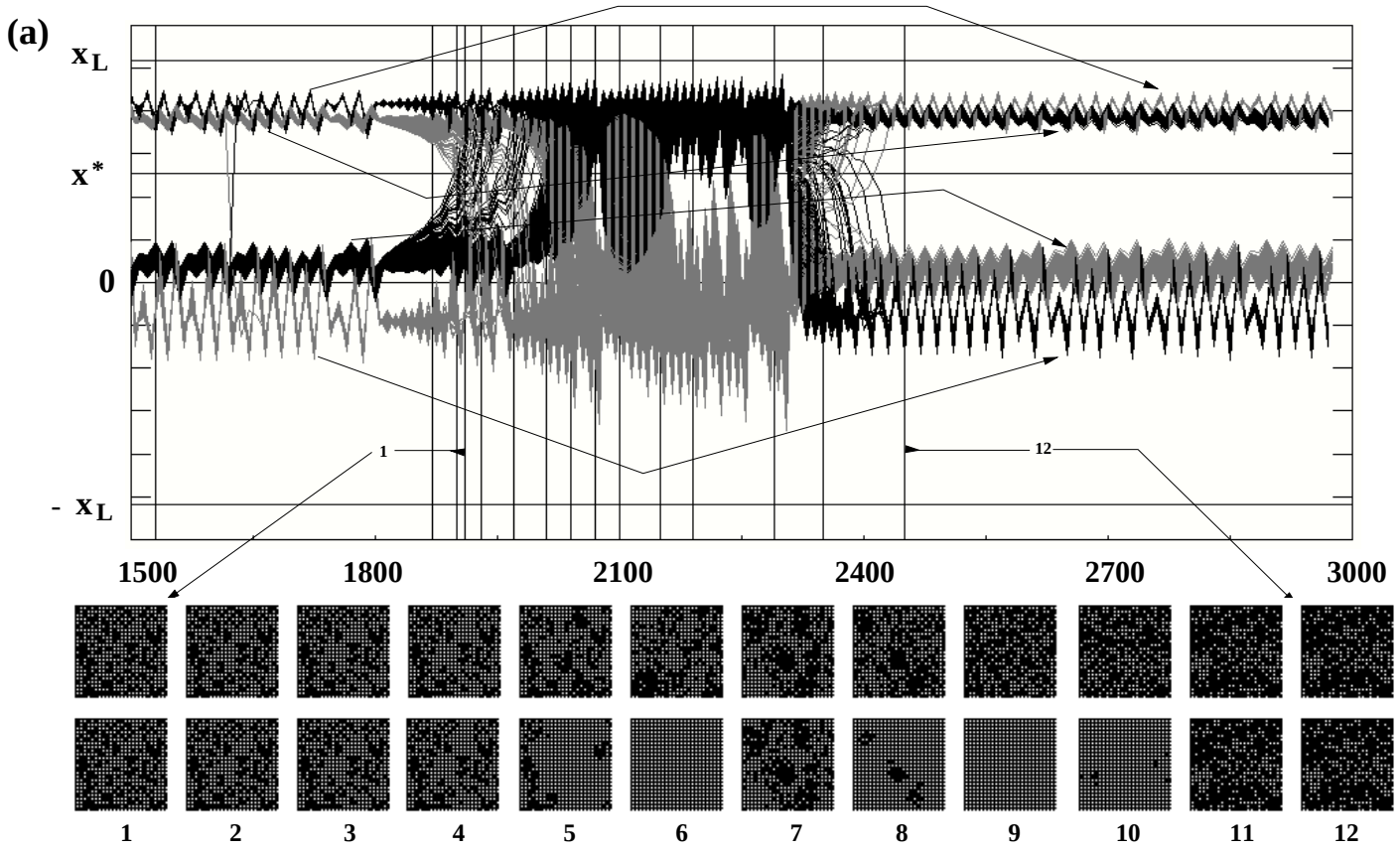
(a)
x_L
x^*
0
$-x_L$
1
12
1500
1800
2100
2400
2700
3000
1
2
3
4
5
6
7
8
9
10
11
12
(b)

Fig 7

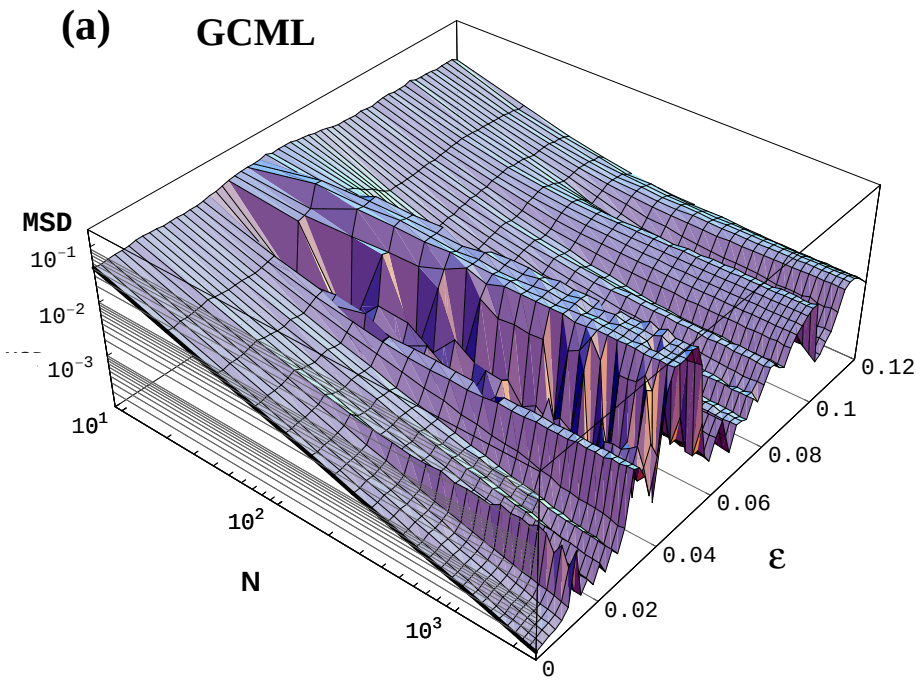
(a)
GCML
MSD
10^{-1}
10^{-2}
10^{-3}
10^{1}
10^{2}
N
10^{3}
0
0.02
0.04
0.06
0.08
0.1
0.12
ε

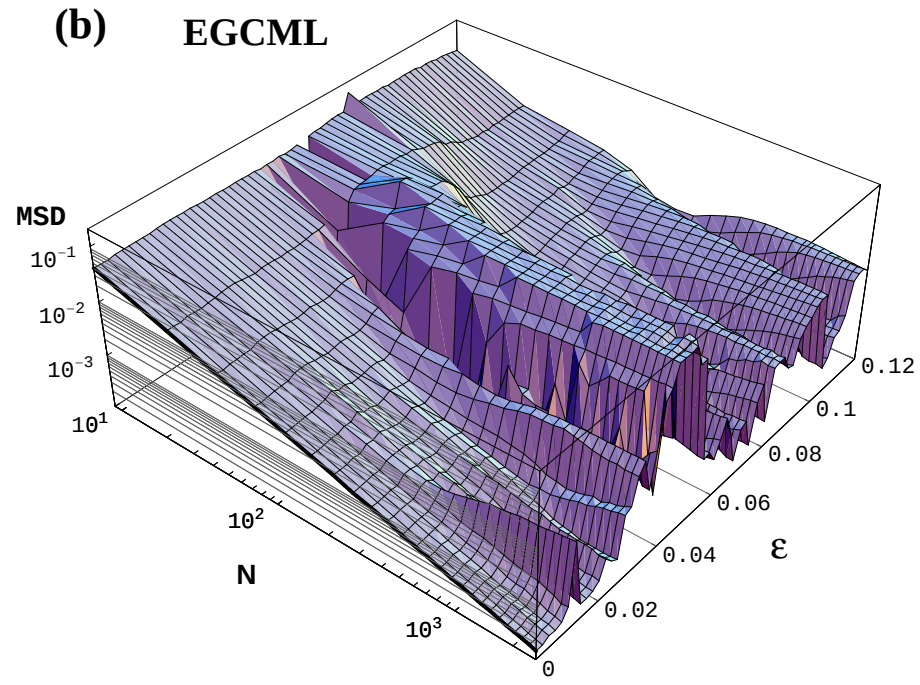
(b)
EGCML
MSD
10^{-1}
10^{-2}
10^{-3}
10^{1}
10^{2}
N
10^{3}
0
0.02
0.04
0.06
0.08
0.1
0.12
ε

Fig. 8

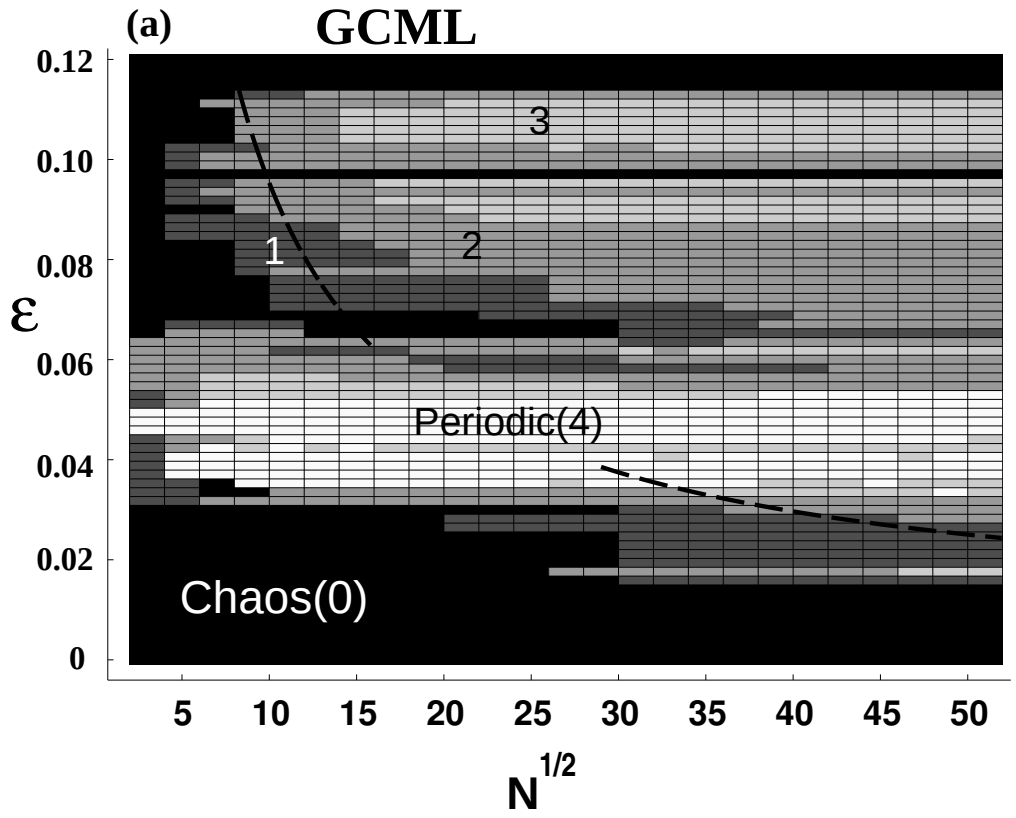
(a)
GCML
0.12
0.10
0.08
0.06
0.04
0.02
0
ε
3
2
1
Periodic(4)
Chaos(0)
5
10
15
20
25
30
35
40
45
50
N^1/2

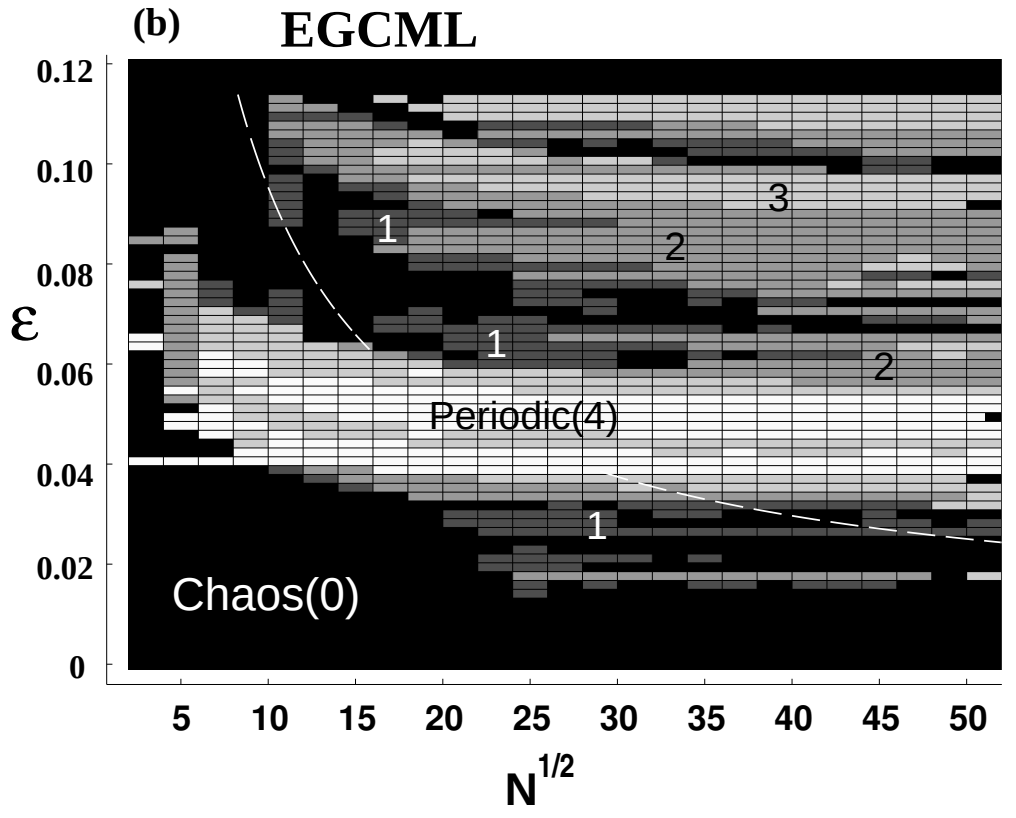
(b)
EGCML
0.12
0.10
0.08
0.06
0.04
0.02
0
ε
3
2
1
1
2
Periodic(4)
1
Chaos(0)
5
10
15
20
25
30
35
40
45
50
N^1/2

Fig. 9

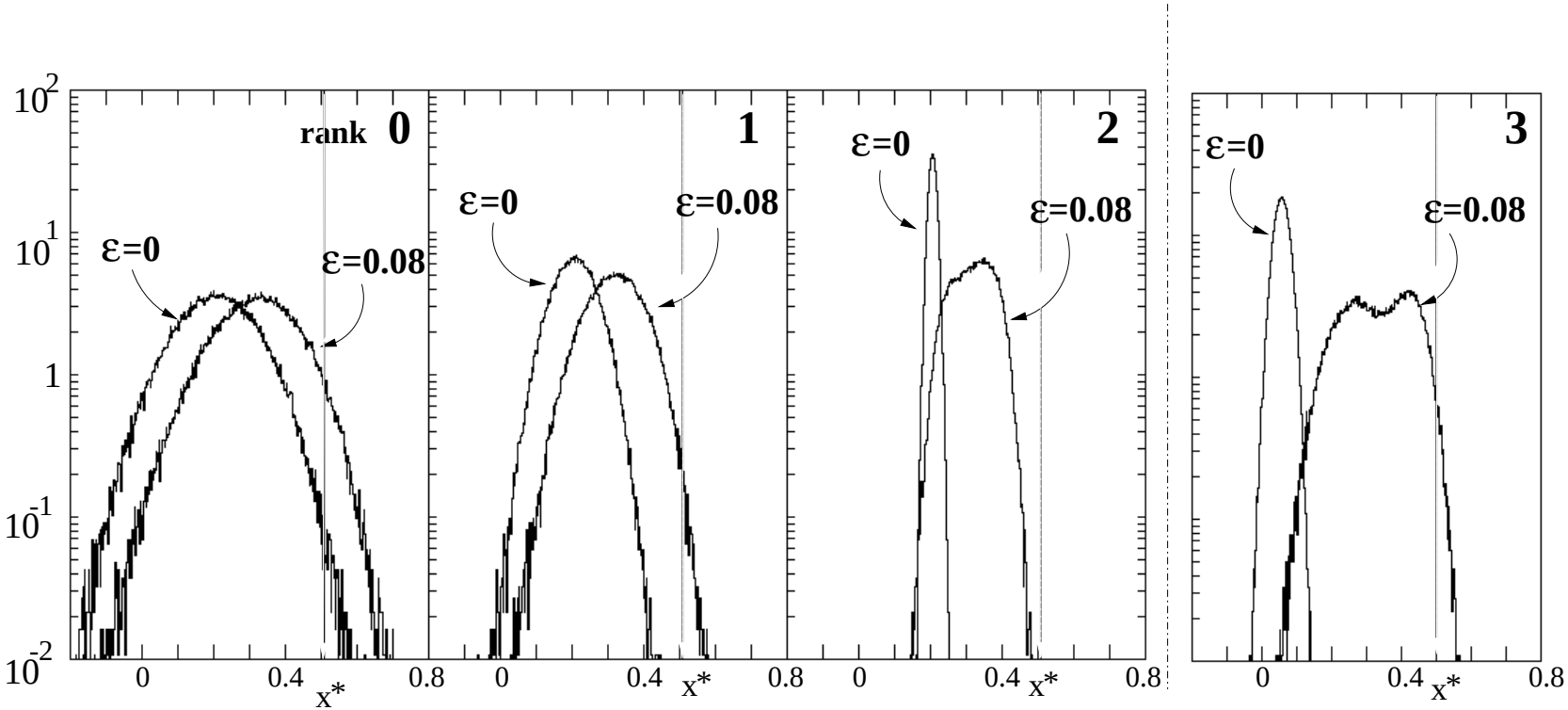

Fig.10

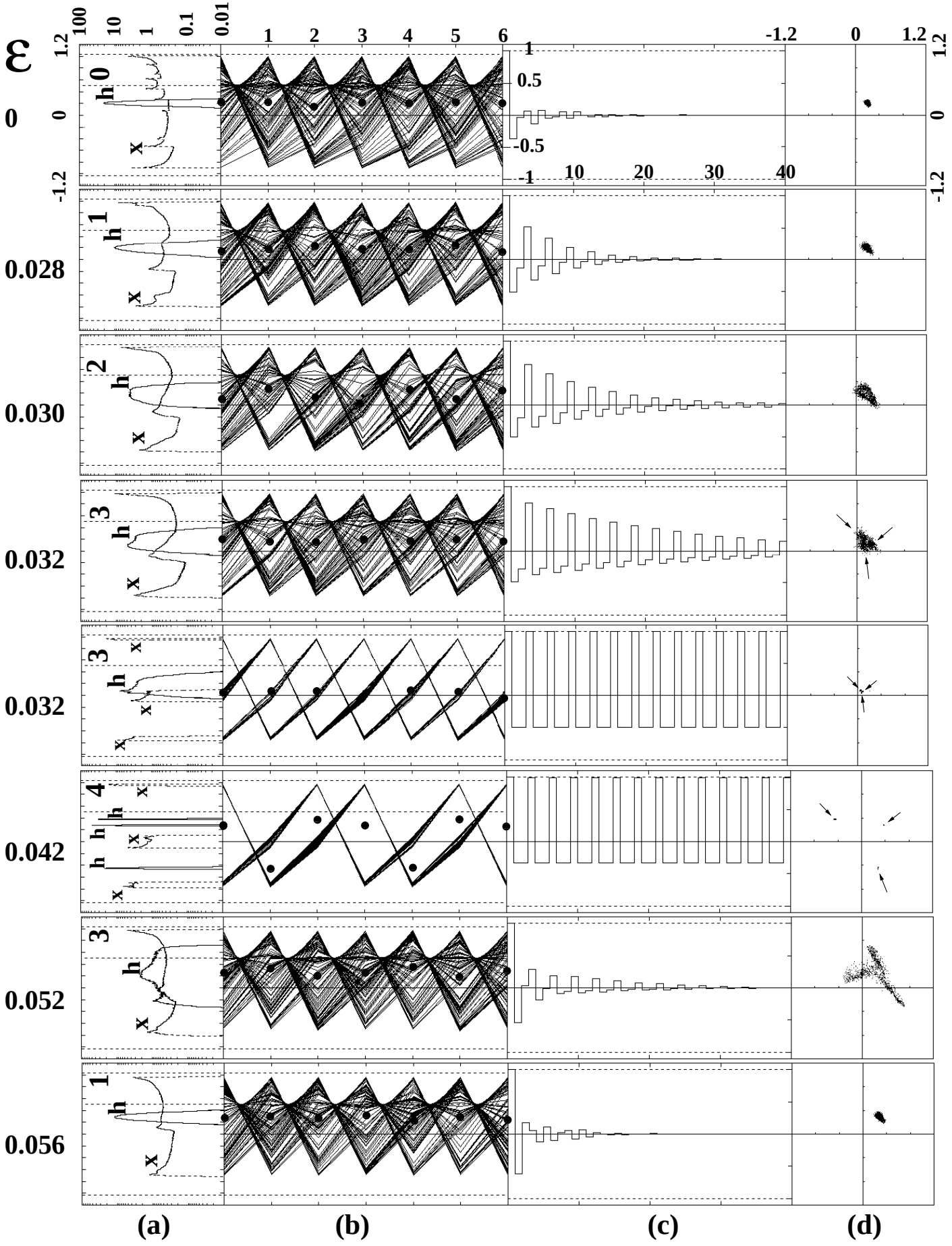
ε
0
0.028
0.030
0.032
0.032
0.042
0.052
0.056
100
10
1
0.1
0.01
1
2
3
4
5
6
-1.2
0
1.2
1
0.5
-0.5
-1
10
20
30
40
h
x
(a)
(b)
(c)
(d)

Fig.11